ISBN 0-315-56076-2

PARAMETRIC STUDY OF ROTOR-BEARING-PEDESTAL SYSTEM USING COMPONENT MODE SYNTHESIS

Aliakbar A. Amini

A Thesis

in

the Department

of

Mechanical Engineering

Presented in Partial Fulfillment of the Requirements
for the Degree of Master of Engineering at
Concordia University
Montreal, Quebec, Canada

January 1990

ABSTRACT

Parametric Study of
Rotor-Bearing-Pedestal System
Using
Component Mode Synthesis

Aliakbar Amini

The thesis is concerned with a study on the dynamic response of rotors supported on flexible pedestals. After a brief review of the current literature, the component mode synthesis method is selected as the appropriate method for studying the response of the rotor-bearing-pedestal system. To enable this study, a computer program **SETSA** is developed. The accuracy of the results obtained by the program is established with respect to standard examples. The computer program is then employed to perform a parametric study of the influence of pedestal stiffness on the rotor dynamic response. Some useful conclusions are obtained from the study and suggestions for future research are indicated.

ACKNOWLEDGEMENT

The author wishes to express his warmest gratitude to Dr. T. S. Sankar for his encouragement and guidance throughout this investigation. Thanks are also due to Drs. Kumar and Ramu for their valuable comments.

Many thanks are due to Mr. Panah for his advise in computer organization, debugging and subroutine suggestions and to Mr. Shahabi for his help in preparation of the manuscript of this thesis.

The author is indebted to his parents for their faith and to Janina Warzecha, who is an excellent mother to my daughters Setarah and Sahar, for her understanding and support.

Finally the support of the Natural Sciences and Engineering Research Council under the grant No. OG 7104 awarded to Dr. Sankar is gratefully acknowledged.

TABLE OF CONTENTS

LIST OF FIGURES

LIST OF TABLES

NOMENCLATURE

$\underset{\sim}{A}$	Partitioned coefficient matrix first order form
$\underset{\sim}{\mathcal{A}}$	First order modally transformed coefficient matrix
B	Rotational degree of freedom in y direction
$\underset{\sim}{B}$	Partitioned coefficient matrix first order form
$\underset{\sim}{\mathcal{B}}$	First order modally transformed coefficient matrix
$\underset{\sim}{C}$	Damping matrix
$\underset{\sim}{D}$	Matrix of dynamical eigenvalue problem
$\underset{\sim}{\hat{D}}$	System matrix of dynamical eigenvalue problem
E	Modulus of elasticity
$\tilde{F}$	Force vector in second order form
$\tilde{\mathcal{q}}$	System modal synthesis state vector
$\tilde{h}$	State vector before partitioning
$\underset{\sim}{I}$	Identity matrix
$\underset{\sim}{K}$	Stiffness matrix
$\underset{\sim}{\mathcal{k}}$	Reordering transformation matrix
ℓ_1, ℓ_2	Disk location
ℓ	Element length
$\underset{\sim}{M}$	Mass matrix
$\underset{\sim}{\mathring{M}}$	Diagonal matrix of biorthogonality
N	Number of elements
$\underset{\sim}{\mathring{N}}$	Diagonal matrix of biorthogonality
$\tilde{\mathcal{P}}$	Modally synthesized force vector
$\tilde{q}$	Synthesized mode state vector
$\tilde{Q}$	Partitioned force vector
t	Time, thickness

$\underset{\sim}{U}$	Matrix of constrained right vector
V	Absolute lateral displacement coordinate in y direction
W	Absolute lateral displacement coordinate in z direction
$\tilde{x}$	Physical displacement coordinates
$\tilde{y}$	State vector partitioned
$\underset{\sim}{Y}$	Constraint matrix left vector
y_0	Right eigenvector
z_0	Left eigenvector
$\underset{\sim}{Z}$	Constrained matrix left vector
$\underset{\sim}{\bar{\alpha}}$	Second reordering transformation matrix applied to first order form
$\hat{\alpha}$	Inverse of eigenvalue, damping exponent of system eigenvalue
$\underset{\sim}{\alpha}$	First reordering transformation matrix applied to second order equation.
$\underset{\sim}{\beta}$	Modal transformation matrix right vector
$\underset{\sim}{\chi}$	Component transformation matrix
Γ	Rotational degree of freedom in z direction
$\tilde{\zeta}$	Vector of modal force
$\tilde{\eta}$	Vector of modal coordinate
λ	Eigenvalue
$\underset{\sim}{\mathring{\Lambda}}$	Diagonal matrix of eigenvalue first order form
ρ	Density
$\underset{\sim}{\psi}$	Displacement static constraint matrix
$\underset{\sim}{\Psi}$	Displacement constraint matrix first order form
ω	Whirl speed

Ω Spin speed

Subscripts

B	Bending
d	Disk
p	Partitioned, Pedestal
R	Retained
r	Rotational
s	System
t	Translational
T	Truncated

Superscripts

B	Boundary
e	Element
i	Index
I	Interior
k	Index, kth component
T, T	Transpose

CHAPTER 1

INTRODUCTION

1.1 General Objective

Whenever power is transmitted from one point to another, for example, in industrial machines such as steam and gas turbines, turbo-generators, internal combustion engines, compressors, transmissions, etc., rotating shafts are used. Flexible rotors are generally composed of concentrated masses such as disks, impellers, rotor segments with distributed mass and elasticity and bearings. Generally ball, roller, or journal bearings are used. High speed heavy rotor systems such as generator rotors are normally supported on fluid film bearings.

Fluid film bearings commonly used in heavy rotating machines are in fact nonlinear in their mechanical behavior. Since the rotors operate well beyond their critical speed regions, the response behavior of the rotors can be predicted using a linear model. It is, therefore, reasonable to consider linear models of the bearing supports to analyze the rotor-bearing behavior.

Due to the increasing demand for improved performance of high speed rotating machinery in various fields such as those used in process equipment, auxiliary power machinery, helicopter technology and nuclear applications, the engineer is faced with the problem of designing a unit capable of smooth operation under various conditions of speed and load. In many of these applications of rotor-bearing systems, achieving an acceptable performance with stable, low level amplitude of vibration is extremely difficult. Therefore while designing a rotor-bearing system, several aspects such as critical speeds, peak unbalanced response, regions of change in whirl directions, and instability must be considered.

The bearing support has a significant effect on the behavior of the system. A support model is complete if it includes such pedestal properties as mass, stiffness and damping. An analysis technique which can appropriately include all these factors is, therefore, an essential component of rotor design.

Finite element techniques are convenient and widely used to model complex rotor-bearing systems consisting of several disks, impellers or mechanical couplings. The finite element method may need a large number of degrees of freedom and require the solution of a large order set of linear equations. In addition to this, the solution of these equations may require the use of time consuming algorithms which may not be economically feasible. There exist a few reduction methods such as Guyan reduction, modal condensation, and component mode synthesis (CMS) by which the size of the system matrices can be reduced. In this thesis the component mode synthesis reduction method is adopted. This technique permits significant reduction in the size of the overall system problem while retaining the essential dynamic characteristics of the structure.

The objective of the present investigation is primarily to develop an efficient and economical method to obtain certain characteristics describing the dynamic response of rotor-bearing-pedestal system based on component mode synthesis reduction technique. Employing this procedure the size of the matrices for the state variables can be considerably reduced without affecting the dynamic characteristic of the system response. The focus of this study is directed towards the development of the digital computer program **SETSA** to perform such an analysis for rotor-bearing-pedestal system based on component mode synthesis. The program **SETSA** is formulated to provide a quick evaluation of the natural frequencies of the system. Finally the computer program **SETSA** is employed to perform a detailed parametric study of a number of system properties of the rotor-bearing-pedestal arrangement. The thesis is also examines the effect of truncation of modes of different orders on the accuracy of the solution through specific examples.

1.2 Literature Review

Dynamic analysis of rotor-bearing system analysis began in early 1919 with the pioneering work by Jeffcotte [1], an English physicist who provided a clear analysis for a particular simple idealization of flexible rotors. He was the first person who successfully explained the whirling phenomena which is probably the most important common type of vibration in rotating shafts caused by unbalance. The resulting equations of motion were solved by direct method.

In 1945 Prohl [2] extended this method and presented the first calculation of synchronous whirling of complex shafts consisting of variable shaft sections with multiple disks. Prohl's method, which is sometimes referred to as the Myklestad-Prohl method, is still considered as one of the best in the general class of transfer matrix method and also one the most practical and widely used solution schemes for today's complex rotor-bearing systems.

Lemke and Trumpler [3] used Prohl's rotor to demonstrate the significant effect of coupling on the response characteristics of the rotor set. Bishop and Parkinson [4] provided a comprehensive review of flexible-rotor analysis based on Jeffcotte's formulation with an emphasis on flexible-rotor balancing.

Modal analysis is another solution procedure which is widely used today to study the behavior of rotor-bearing systems. Lund [5] used biorthogonality relation to study the dynamics of flexible rotors in fluid film bearing. Bhat, Subbiah and Sankar [6] applied modal analysis to determine the dynamic response of the rotor supported on dissimilar hydrodynamic bearings. The dissimilarity occurred due to different clearances and different loads on the bearing.

Finite element method is also a convenient technique to model complex rotor-bearing systems, which may consist of several disks, impellers or mechanical couplings, etc. Ruhl and Brooker [7] used finite element method to evaluate the dynamic characteristics of the rotor. Their approach was based on the consistent mass formulation of Archer [8] which provides for a more accurate modeling with less degrees of freedom.

Nelson and McVaugh [9] included the effect of rotary inertia, gyroscopic moments, and axial load to Ruhl's finite element model to calculate the natural whirl speeds and unbalance response of a typical overhung system. They also presented a coordinate reduction procedure to model elements with variable cross-section properties. In addition, the finite element equation of motion is presented in both fixed and rotating reference frames.

Subsequent studies [10,11,12] included the effects of internal damping, axial torque, hysteresis damping, etc., in modeling the rotor-bearing system using finite element method. Guyan's [13] reduction technique was used to reduce the size of the assembled finite element matrices, since it was difficult to handle them on digital computer.

Past research has shown that modal analysis of the structural finite element model is a vital part of the dynamic analysis of structure. Large structures such as airplanes may consist of several components, each of which may be manufactured by different organizations. The analysis of each component may require a large number of degrees of freedom finite element model. The assembled structure may therefore contain so many degrees of freedom that it cannot be economically handled on the largest of modern computers. It is, therefore, essential to seek a method to overcome this difficulty.

Utilizing the component mode synthesis technique, each component is analyzed separately and the size of the matrices is reduced by truncating the unwanted degrees of freedom. The reduced components are then assembled to form a complete structure which can be handled more easily by modern computers. Component mode synthesis allows for substantial reduction in the size of the overall system while still retaining the essential dynamic characteristics. This reduction accounts for reduced computer time and reduced cost for analysts.

Component mode synthesis has been extensively developed over the past 25 years. The trend in structural analysis towards the modeling of structural systems by component mode synthesis or substructure coupling started by considering the dynamic analysis of lightly damped system with symmetric property matrices. The solution of such a system as airframes, buildings, bridges, etc., leads to real eigen-value problem. More general analysis is required for structures such as those with rotating parts or non-proportional damping which leads to complex eigenvalue problem.

The development of the component mode synthesis technique was first credited to Hurty [14,15]. The technique was highly suitable for the analysis of structural system with redundant interfaces. The structure may be divided into several components. The displacement of the components is defined in terms of generalized coordinates that are related to specified sets of normalized displacement modes such as rigid-body, constraint and normal modes.

Gladwell [16], who can also be considered an early pioneer in the component mode synthesis, proposed branch mode analysis to calculate the natural frequencies and principle modes of free undamped vibration for a system with many degrees of freedom. In this method each component of a complex continuous vibrating system is replaced by an appropriate lumped mass model.

A comprehensive survey (culminating in 1975) was conducted by Craig and Chang [17]. This paper reviewed the majority of methods presented in the literature. The main objective of the researchers was to improve the results of the undamped symmetric component mode or substructure synthesis which, in fact, raised two important questions: (i) how to select a set of component mode, and (ii) how to enforce the geometric compatibility at the interface between the two components.

Hurty's method [15], later modified by Craig and Bampton [18], was formulated for lightly damped symmetric coefficient second order component mode system. Hurty neglected the damping term in his analysis and this resulted in real eigenvalue and eigenvector. The full modal transformation method suggested by Craig and Bampton is a superposition of fixed boundary mode plus component constraint mode. Hurty improved the analysis by adding the structural damping factor in the normal mode response equation of motion.

Robin [19], Kuhar and Stahle [20], and Hintz [21] improved the component modal representation by suggesting many different procedures which permit valuable information from truncated high frequency modes to be incorporated into the retained mode in an approximated way. For example, Robin included free boundary modes and residual effects including inertial and dissipative contribution; whereas, Kuhar introduced dynamic transformation into the formulation. He believed that fixed boundary plus constrained modes tend to have the best convergence.

Complex modal analysis to the second order system was first developed by Hasselman and Kaplan [22]. The analysis accounted for any arbitrary constant coefficients which lead to complex eigenvalues and eigenvectors. They did not include constraint modes in their study. Therefore, contrary to Craig and Bampton [18] it does not provide a full modal transformation.

Glasgow [23] presented a significant study on complex mode synthesis allowing for a full modal transformation. The modal synthesis is valid for a broad range of second order constant coefficient differential equations which may involve general nonsymmetric velocity and/or displacement dependent terms. The equations of motion were solved for whirl mode, stability and general forced motion response.

Craig and Chung [24] improved Hasselman and Kaplan's initial work by using Hamiltonian first order differential equation incorporating Rayleigh dissipation function to formulate a procedure for damped system.

Vibration analysis of multiple component synthesis method was also reviewed by Massaki and Akio [25]. In this investigation, which is an extension to the method of Banfield and Hruda [26], the authors substantially reduced the size of matrices and compared the results of the analysis with those of finite element method. The accuracy of the calculation was as high as that of finite element method but with less CPU time. In this analysis damping was neglected.

Subsequent study by Meirovitch and Hale [27,28] presented a different procedure, other than component mode synthesis, to improve discrete substructure representation in dynamic synthesis. Meirovitch and Hale suggested that in the presence of the Rayleigh-Ritz method, the motion of each component mode can be replaced by a complete set of admissible function and the component modes need not be developed. Admissible function can be selected from low order polynomials which are computationally easier to handle. Components are coupled by imposing approximate geometric compatibility by means of the method of weighted residuals.

A method of calculating eigenvalues for gyroscopic system was also presented by Meirovitch [29]. The analysis dealt with transforming the skew symmetric matrices which can be easily used in modal transformation. This can be well adapted to either symmetric undamped or purely gyroscopic rotating structural systems.

Zheng [30] and others reviewed the gyroscopic mode synthesis including such aspects as the effect of nonlinearity and asymmetricity of bearings, gyroscopic moments of shafts and disks, and damping. By extending the Meirovitch [29] analysis, the authors concluded two important advantages of the gyroscopic mode synthesis: (i) real mode programs can be used for the calculation of gyroscopic modes in component mode synthesis without the use of biorthogonality relation to decouple the equation of motion. This in effect saves computer time and memory, and is in contrast to the analysis conducted by Glasgow and Nelson [31] and Nelson and Meacham [32]; (ii) the synthesis equation of the system is an asymmetric matrix equation with real coefficients.

Craggs [33] has contributed substantially to the dynamic analysis of turbo-generators. Component mode synthesis was used to reduce the size of the finite element matrices. In a similar procedure suggested by Morton [34] the components included rotor assembly, bearing and foundation. The approach presented two advantages: (i) each component can be analyzed separately and important information can be retained, and (ii) the components are related to an actual physical entity so that predicted properties can be compared with the measured ones.

Rotor-bearing foundation system was analyzed by many other researchers using component mode synthesis. Gong [35], for example, neglected lateral damping and gyroscopic effect to analyze the dynamics of large steam turbine-generator rotor-bearing- foundation system. The structure was divided into two components, the rotor and the foundation. The oil film bearing was used as a connector between the rotor and foundation.

Kramer [36] applied a different procedure to calculate the unbalance vibration of rotor-foundation system. The author reduced the computational expenses to an acceptable level by first calculating the dynamic stiffness of the foundation, then incorporating the influence of the foundation on the rotor by the dynamic stiffness of the foundation at the connecting points to the rotor.

Subbiah [37] included pedestal mass in his finite element rotor-bearing-pedestal system to calculate the response of the system. In his study, modal condensation was used to reduce the size of the matrices and the effect of damping was neglected. As is clearly reflected in the literature, there are three different mode synthesis methods that can be applied to mode synthesis development. Depending on the boundary condition imposed at the interface between the two components, these methods can be classified as: (i) fixed-interface mode synthesis, (ii) free interface mode synthesis method, and (iii) loaded interface mode synthesis method.

1.3 Scope And Layout of Thesis

From the foregoing it is clear that the component mode synthesis method is very appropriate for the analysis of the rotor dynamic problem. In addition to the advantage of significant reduction in computational effort, it is also consistent with the physical reality that the total response of the system is composed of the responses of the individual components. Therefore, in this thesis, the component mode synthesis method is developed to perform the parametric study of rotor-bearing-pedestal system.

In chapter 2, the component mode synthesis method as well as all the relevant equations are formulated. Based on this formulation a digital computer program named SETARAH-SAHAR, herein referred to as **SETSA** is developed. Chapter 3 contains a complete description of the computer program for implementation of component mode synthesis method using **Cyber1** computer system followed by program flow-charts and subroutine descriptions. The accuracy of the program is established with the use of several examples. The computer program **SETSA** is employed in chapter 4 to provide a detailed analysis of Jeffcotte's rotor supported on flexible pedestals. Detailed numerical study of the influence of rotor-bearing-pedestal characteristics on the critical speed of the rotor is presented. Finally, the thesis ends with a discussion on some of the conclusions presented and some recommendations for future research endeavours.

CHAPTER 2

COMPONENT MODE SYNTHESIS

2.1 Introduction

The successful design of structures requires a comprehensive study of dynamic analysis before the structure is placed in its operating environment. A vital part of this effort is the modal analysis of structural finite element models. In the classical approach, it is usual to determine normal modes and auxiliary static analysis directly from the finite element model. However, modern structural systems have become very complex and major components are often manufactured by different organizations. It is, therefore, often difficult to assemble an entire finite element model in a timely manner. In addition, many finite element models may contain so many degrees of freedom that they cannot be directly handled on the largest of modern computers. For these reasons, it is desirable to develop methods for analyzing substructures of a finite element model. Such an analysis has come to be known as component mode synthesis in dynamic analysis and substructuring in static analysis.

Component mode synthesis allows for significant reduction in the size of the overall system problem while retaining the essential dynamic characteristics. The coordinates of the component are classified as boundary coordinates if they are common to two or more components and interior coordinates if they do not interface with any other component. It is desirable that component mode synthesis techniques for the dynamic analysis of structures have the following characteristics:

1. Computational efficiency: the component mode representation should contain a minimum number of dependent degrees of freedom or modes for each component.
2. Interchangeability: the component mode set should be independent of the inertial and stiffness properties of adjacent components. Such a component mode set may be used interchangeably in different structural systems with compatible interface.
3. Component flexibility: the method should permit optional interface degree of freedom in a component mode set that may be used or discarded at the time of synthesis.
4. Synthesis flexibility: the synthesis technique should not be constrained to a particular type of component mode set. The synthesis technique should be amenable to accepting different types of component mode sets, for example, fixed interface, free interface, inertial loading, etc.
5. Modal acceleration analysis: static solution for

the synthesized system, which may be required for modal acceleration forced response analysis, should be available. Such static analysis should be available regardless of the complexity of component interfaces, without requiring the assembly of a system finite element model.

The constrained normal mode is found by fixing all boundary coordinates and determining the free vibration modes of the constrained component. It is these modes that provide for the reduction of the number of degrees of freedom system.

The constraint modes are determined by giving each of the boundary coordinates a unit displacement, in turn, fixing all other boundary coordinates and allowing the internal coordinates to displace.

When the constraint modes and constrained normal modes are obtained then each component is transformed in terms of its constrained normal mode and assembled into a lower order set of system equation. This reduced order set of system equation is then used to obtain system free and forced response.

2.2 Analytical Development

The analytical development here will cover the complete development of the system equations of motion using component mode synthesis. This technique allows each component to be restructured in terms of two types of component modes, namely constraint modes (static) and constrained normal mode (dynamic). It is the constrained normal mode which is responsible for the reduction size matrices of the system. By this method the influence of pedestal flexibility on rotor critical speed will be analyzed. The typical rotor-bearing to be simulated as illustrated in Fig.2.2.1 is modeled as an assemblage of discrete disks, rotor segments with distributed mass and elasticity, and discrete bearings. The rotor can be divided into several components, each component may be composed of several finite elements. It is often difficult to assemble the entire finite element model in a timely manner.

Utilizing the component mode synthesis technique, each component is analyzed separately, and the size of the component matrices is reduced by mode truncation. The reduced size of all the components are then assembled to form the system assembly, which is economically feasible and easy to handle. The finite element equation of motion, constant coefficient of component (κ) can be written as:

$$\underset{\sim}{M}^{(\kappa)}\ddot{\tilde{X}}^{(\kappa)} + \underset{\sim}{C}^{(\kappa)}\dot{\tilde{X}}^{(\kappa)} + \underset{\sim}{K}^{(\kappa)}\tilde{X}^{(\kappa)} = \tilde{F}^{(\kappa)}(t) \qquad (2.1)$$

To establish component mode development, first the displacement vector $\tilde{X}$ is partitioned into boundary $\tilde{X}^{B}$ and

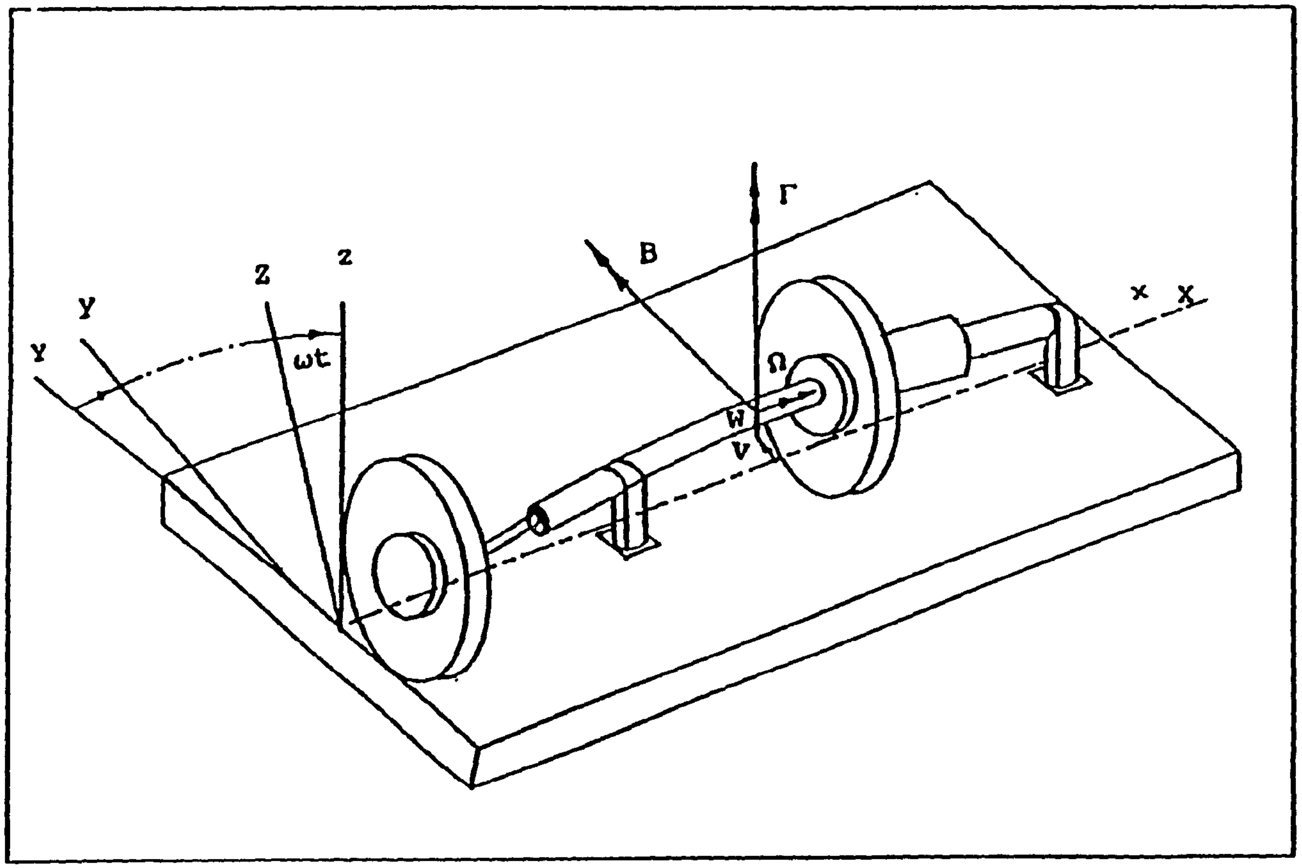

Fig.2.2.1 Typical system configuration [10]

interior $\tilde{X}^I$ coordinates. The superscript (κ) is omitted for simplicity. Then the coordinate reordering transformation $\underset{\sim}{\alpha}$ is applied to the equation (2.1) such that:

$$\tilde{X} = \underset{\sim}{\alpha}\, \tilde{X}_p \tag{2.2a}$$

where

$$\tilde{X}_p = \begin{Bmatrix} \tilde{X}_p^B \\ \tilde{X}_p^I \end{Bmatrix} \tag{2.2b}$$

Substituting equation (2.2a) into equation (2.1) and premultipling by $\underset{\sim}{\alpha}^T$ to obtain:

$$\underset{\sim}{\alpha}^T \underset{\sim}{M}\, \underset{\sim}{\alpha}\, \ddot{\tilde{X}}_p + \underset{\sim}{\alpha}^T \underset{\sim}{C}\, \underset{\sim}{\alpha}\, \dot{\tilde{X}}_p + \underset{\sim}{\alpha}^T \underset{\sim}{K}\, \underset{\sim}{\alpha}\, \tilde{X}_p = \underset{\sim}{\alpha}^T \tilde{F}\ (t) \tag{2.3}$$

which in partitioned form, the equation (2.3) will become:

$$\begin{bmatrix} \underset{\sim}{M}^{BB} & \underset{\sim}{M}^{BI} \\ \underset{\sim}{M}^{IB} & \underset{\sim}{M}^{II} \end{bmatrix} \begin{Bmatrix} \ddot{\tilde{X}}_p^B \\ \ddot{\tilde{X}}_p^I \end{Bmatrix} + \begin{bmatrix} \underset{\sim}{C}^{BB} & \underset{\sim}{C}^{BI} \\ \underset{\sim}{C}^{IB} & \underset{\sim}{C}^{II} \end{bmatrix} \begin{Bmatrix} \dot{\tilde{X}}_p^B \\ \dot{\tilde{X}}_p^I \end{Bmatrix} +$$

$$\begin{bmatrix} \underset{\sim}{K}^{BB} & \underset{\sim}{K}^{BI} \\ \underset{\sim}{K}^{IB} & \underset{\sim}{K}^{II} \end{bmatrix} \begin{Bmatrix} \tilde{X}_p^B \\ \tilde{X}_p^I \end{Bmatrix} = \underset{\sim}{\alpha}^T \begin{Bmatrix} \tilde{F}_p^B \\ \tilde{F}_p^I \end{Bmatrix} \tag{2.4}$$

or

$$\underset{\sim}{M}_p \ddot{\tilde{X}}_p + \underset{\sim}{C}_p \dot{\tilde{X}}_p + \underset{\sim}{K}_p \tilde{X}_p = \tilde{F}_p(t) \tag{2.5}$$

The component mode development can proceed directly using first or second order form. Though the two techniques are equivalent, it is usually more convenient to write the equations of motion in first order, or state space form. In the following formulation the first order development is adopted in detail.

2.2.1 First Order Development

The displacement vector of equation (2.4) can be used to construct the related state vector. Using this state vector the component equation of motion (2.5) can be written in first order form as follows:

$$\begin{bmatrix} \underset{\sim}{0} & \underset{\sim}{M}_P \\ \underset{\sim}{M}_P & \underset{\sim}{C}_P \end{bmatrix} \dot{\tilde{h}} + \begin{bmatrix} -\underset{\sim}{M}_P & \underset{\sim}{0} \\ \underset{\sim}{0} & \underset{\sim}{K}_P \end{bmatrix} \tilde{h} = \begin{Bmatrix} \tilde{0} \\ \tilde{F}_P \end{Bmatrix} \tag{2.6}$$

where the state vector is written as follows:

$$\tilde{h} = \begin{Bmatrix} \dot{\tilde{X}}_P \\ \tilde{X}_P \end{Bmatrix} = \begin{Bmatrix} \dot{\tilde{X}}_P^B \\ \dot{\tilde{X}}_P^I \\ \tilde{X}_P^B \\ \tilde{X}_P^I \end{Bmatrix} \tag{2.7}$$

For simplicity the subscript P will be omitted and by using $\underset{\sim}{\overline{\alpha}}$ transformation to equation (2.6), all boundaries and interior terms can be collected such that:

$$\tilde{h} = \underset{\sim}{\overline{\alpha}}\, \tilde{y} \tag{2.8a}$$

where

$$\bar{\underset{\sim}{\alpha}} = \begin{bmatrix} \underset{\sim}{I} & \underset{\sim}{0} & \underset{\sim}{0} & \underset{\sim}{0} \\ \underset{\sim}{0} & \underset{\sim}{0} & \underset{\sim}{I} & \underset{\sim}{0} \\ \underset{\sim}{0} & \underset{\sim}{I} & \underset{\sim}{0} & \underset{\sim}{0} \\ \underset{\sim}{0} & \underset{\sim}{0} & \underset{\sim}{0} & \underset{\sim}{I} \end{bmatrix} \tag{2.8b}$$

and

$$\tilde{y} = \begin{Bmatrix} \tilde{y}^B \\ \tilde{y}^I \end{Bmatrix} = \begin{Bmatrix} \dot{\tilde{X}}^B \\ \tilde{X}^B \\ \dot{\tilde{X}}^I \\ \tilde{X}^I \end{Bmatrix} \tag{2.8c}$$

Substituting equation (2.8a) into (2.6) and premultiplying by $\bar{\underset{\sim}{\alpha}}^T$ the equation (2.6) in expanded form will become:

$$\begin{bmatrix} \underset{\sim}{I} & \underset{\sim}{0} & \underset{\sim}{0} & \underset{\sim}{0} \\ \underset{\sim}{0} & \underset{\sim}{0} & \underset{\sim}{I} & \underset{\sim}{0} \\ \underset{\sim}{0} & \underset{\sim}{I} & \underset{\sim}{0} & \underset{\sim}{0} \\ \underset{\sim}{0} & \underset{\sim}{0} & \underset{\sim}{0} & \underset{\sim}{I} \end{bmatrix}^T \begin{bmatrix} \underset{\sim}{0} & \underset{\sim}{0} & \underset{\sim}{M}^{BB} & \underset{\sim}{M}^{BI} \\ \underset{\sim}{0} & \underset{\sim}{0} & \underset{\sim}{M}^{IB} & \underset{\sim}{M}^{II} \\ \underset{\sim}{M}^{BB} & \underset{\sim}{M}^{BI} & \underset{\sim}{C}^{BB} & \underset{\sim}{C}^{BI} \\ \underset{\sim}{M}^{IB} & \underset{\sim}{M}^{II} & \underset{\sim}{C}^{IB} & \underset{\sim}{C}^{II} \end{bmatrix} \begin{bmatrix} \underset{\sim}{I} & \underset{\sim}{0} & \underset{\sim}{0} & \underset{\sim}{0} \\ \underset{\sim}{0} & \underset{\sim}{0} & \underset{\sim}{I} & \underset{\sim}{0} \\ \underset{\sim}{0} & \underset{\sim}{I} & \underset{\sim}{0} & \underset{\sim}{0} \\ \underset{\sim}{0} & \underset{\sim}{0} & \underset{\sim}{0} & \underset{\sim}{I} \end{bmatrix} \begin{Bmatrix} \ddot{\tilde{X}}^B \\ \dot{\tilde{X}}^B \\ \ddot{\tilde{X}}^I \\ \dot{\tilde{X}}^I \end{Bmatrix} +$$

$$\begin{bmatrix} \underset{\sim}{I} & \underset{\sim}{0} & \underset{\sim}{0} & \underset{\sim}{0} \\ \underset{\sim}{0} & \underset{\sim}{0} & \underset{\sim}{I} & \underset{\sim}{0} \\ \underset{\sim}{0} & \underset{\sim}{I} & \underset{\sim}{0} & \underset{\sim}{0} \\ \underset{\sim}{0} & \underset{\sim}{0} & \underset{\sim}{0} & \underset{\sim}{I} \end{bmatrix}^T \begin{bmatrix} -\underset{\sim}{M}^{BB} & -\underset{\sim}{M}^{BI} & \underset{\sim}{0} & \underset{\sim}{0} \\ -\underset{\sim}{M}^{IB} & -\underset{\sim}{M}^{II} & \underset{\sim}{0} & \underset{\sim}{0} \\ \underset{\sim}{0} & \underset{\sim}{0} & \underset{\sim}{K}^{BB} & \underset{\sim}{K}^{BI} \\ \underset{\sim}{0} & \underset{\sim}{0} & \underset{\sim}{K}^{IB} & \underset{\sim}{K}^{II} \end{bmatrix} \begin{bmatrix} \underset{\sim}{I} & \underset{\sim}{0} & \underset{\sim}{0} & \underset{\sim}{0} \\ \underset{\sim}{0} & \underset{\sim}{0} & \underset{\sim}{I} & \underset{\sim}{0} \\ \underset{\sim}{0} & \underset{\sim}{I} & \underset{\sim}{0} & \underset{\sim}{0} \\ \underset{\sim}{0} & \underset{\sim}{0} & \underset{\sim}{0} & \underset{\sim}{I} \end{bmatrix} \begin{Bmatrix} \dot{\tilde{X}}^B \\ \tilde{X}^B \\ \dot{\tilde{X}}^I \\ \tilde{X}^I \end{Bmatrix} =$$

$$\begin{bmatrix} \underset{\sim}{I} & \underset{\sim}{0} & \underset{\sim}{0} & \underset{\sim}{0} \\ \underset{\sim}{0} & \underset{\sim}{0} & \underset{\sim}{I} & \underset{\sim}{0} \\ \underset{\sim}{0} & \underset{\sim}{I} & \underset{\sim}{0} & \underset{\sim}{0} \\ \underset{\sim}{0} & \underset{\sim}{0} & \underset{\sim}{0} & \underset{\sim}{I} \end{bmatrix}^T \begin{Bmatrix} \tilde{0} \\ \tilde{0} \\ \tilde{F}^B \\ \tilde{F}^I \end{Bmatrix} \tag{2.9a}$$

which is simplified to:

$$\begin{bmatrix} \underset{\sim}{0} & \underset{\sim}{M}^{BB} & \underset{\sim}{0} & \underset{\sim}{M}^{BI} \\ \underset{\sim}{M}^{BB} & \underset{\sim}{C}^{BB} & \underset{\sim}{M}^{BI} & \underset{\sim}{C}^{BI} \\ \underset{\sim}{0} & \underset{\sim}{M}^{IB} & \underset{\sim}{0} & \underset{\sim}{M}^{II} \\ \underset{\sim}{M}^{IB} & \underset{\sim}{C}^{IB} & \underset{\sim}{M}^{II} & \underset{\sim}{C}^{II} \end{bmatrix} \begin{Bmatrix} \ddot{\tilde{X}}^{B} \\ \dot{\tilde{X}}^{B} \\ \ddot{\tilde{X}}^{I} \\ \dot{\tilde{X}}^{I} \end{Bmatrix} + \begin{bmatrix} -\underset{\sim}{M}^{BB} & \underset{\sim}{0} & -\underset{\sim}{M}^{BI} & \underset{\sim}{0} \\ \underset{\sim}{0} & \underset{\sim}{C}^{BB} & \underset{\sim}{0} & \underset{\sim}{K}^{BI} \\ -\underset{\sim}{M}^{IB} & \underset{\sim}{0} & -\underset{\sim}{M}^{II} & \underset{\sim}{0} \\ \underset{\sim}{0} & \underset{\sim}{K}^{IB} & \underset{\sim}{0} & \underset{\sim}{C}^{II} \end{bmatrix} \begin{Bmatrix} \dot{\tilde{X}}^{B} \\ \tilde{X}^{B} \\ \dot{\tilde{X}}^{I} \\ \tilde{X}^{I} \end{Bmatrix} = \begin{Bmatrix} \tilde{0} \\ \tilde{F}^{B} \\ \tilde{0} \\ \tilde{F}^{I} \end{Bmatrix} \quad (2.9b)$$

or

$$\begin{bmatrix} \underset{\sim}{A}^{BB} & \underset{\sim}{A}^{BI} \\ \underset{\sim}{A}^{IB} & \underset{\sim}{A}^{II} \end{bmatrix} \begin{Bmatrix} \dot{\tilde{y}}^{B} \\ \dot{\tilde{y}}^{I} \end{Bmatrix} + \begin{bmatrix} \underset{\sim}{B}^{BB} & \underset{\sim}{B}^{BI} \\ \underset{\sim}{B}^{IB} & \underset{\sim}{B}^{II} \end{bmatrix} \begin{Bmatrix} \tilde{y}^{B} \\ \tilde{y}^{I} \end{Bmatrix} = \begin{Bmatrix} \tilde{Q}^{B} \\ \tilde{Q}^{I} \end{Bmatrix} \quad (2.9c)$$

or

$$\underset{\sim}{A}\,\dot{\tilde{y}} + \underset{\sim}{B}\,\tilde{y} = \tilde{Q} \quad (2.9d)$$

2.2.2 Constraint Mode

Constraint mode is obtained by unconstraining the interior coordinates and by allowing a unit displacement to boundary coordinates in turn with all the other boundary coordinates fixed. The constraint modes are included to treat redundancies in the interconnection system. These modes will exist only if the system of constraints on the component is indeterminate. The number of constraint modes is equal to the number of redundant constraints. The constraint mode can be developed by considering the static problem of equation (2.4); disregarding subscript p for simplicity, the static mode is shown as follows:

$$\begin{bmatrix} \underset{\sim}{K}^{BB} & \underset{\sim}{K}^{BI} \\ K^{IB} & K^{II} \end{bmatrix} \begin{Bmatrix} \tilde{X}^{B} \\ \tilde{X}^{I} \end{Bmatrix} = \underset{\sim}{\alpha}^{T} \begin{Bmatrix} \tilde{F}^{B} \\ \tilde{0} \end{Bmatrix} \tag{2.10}$$

The interior coordinates can be obtained by considering the second row of the above equation which can result:

$$\underset{\sim}{K}^{IB}\tilde{X}^{B} + \underset{\sim}{K}^{II}\tilde{X}^{I} = 0 \tag{2.11}$$

$$\tilde{X}^{I} = -\left(\underset{\sim}{K}^{II}\right)^{-1}\underset{\sim}{K}^{IB}\tilde{X}^{B} \tag{2.12}$$

or

$$\tilde{X}^{I} = \underset{\sim}{\psi}\,\tilde{X}^{B} \tag{2.13}$$

$$\underset{\sim}{\psi} = -\left(\underset{\sim}{K}^{II}\right)^{-1}\underset{\sim}{K}^{IB} \tag{2.13a}$$

The displacement constraint mode can be shown as:

$$\begin{Bmatrix} \tilde{X}^{B} \\ \tilde{X}^{I} \end{Bmatrix} = \begin{bmatrix} \underset{\sim}{I} \\ \underset{\sim}{\psi} \end{bmatrix} \tilde{X}^{B} \tag{2.14}$$

and the velocity constraint mode is:

$$\begin{Bmatrix} \dot{\tilde{X}}^{B} \\ \dot{\tilde{X}}^{I} \end{Bmatrix} = \begin{bmatrix} \underset{\sim}{I} \\ \underset{\sim}{\psi} \end{bmatrix} \dot{\tilde{X}}^{B} \tag{2.15}$$

Then the component constraint mode in state space form can be constructed using equations (2.14) and (2.15) such that:

$$\tilde{y}^B = \begin{Bmatrix} \dot{\tilde{X}}^B \\ \tilde{X}^B \end{Bmatrix} \tag{2.16}$$

$$\tilde{y}^I = \begin{Bmatrix} \dot{\tilde{X}}^I \\ \tilde{X}^I \end{Bmatrix} \tag{2.17}$$

Collecting the boundary and interior coordinates together such that:

$$\tilde{y} = \begin{Bmatrix} \tilde{y}^B \\ \tilde{y}^I \end{Bmatrix} = \begin{Bmatrix} \dot{\tilde{X}}^B \\ \tilde{X}^B \\ \dot{\tilde{X}}^I \\ \tilde{X}^I \end{Bmatrix} = \begin{bmatrix} \underset{\sim}{I} & \underset{\sim}{0} \\ \underset{\sim}{0} & \underset{\sim}{I} \\ \underset{\sim}{\psi} & \underset{\sim}{0} \\ \underset{\sim}{0} & \underset{\sim}{\psi} \end{bmatrix} \begin{Bmatrix} \dot{\tilde{X}}^B \\ \tilde{X}^B \end{Bmatrix} \tag{2.18a}$$

they can be written in forms of boundary coordinates only as:

$$\tilde{y} = \begin{Bmatrix} \tilde{y}^B \\ \tilde{y}^I \end{Bmatrix} = \begin{bmatrix} \underset{\sim}{I} \\ \underset{\sim}{\Psi} \end{bmatrix} \tilde{y}^B \tag{2.18b}$$

where

$$\underset{\sim}{\Psi} = \begin{bmatrix} \underset{\sim}{\psi} & \underset{\sim}{0} \\ \underset{\sim}{0} & \underset{\sim}{\psi} \end{bmatrix} \tag{2.18c}$$

2.2.3 Constraint Normal Mode

The constraint normal mode of the component defines the displacement relative to the connections. It describes the motion of the interior coordinates with all constraints fixed. The constrained normal mode is often called the "fixed-constraint normal mode" or simply the "normal mode" for brevity. It is obtained by setting all boundary coordinates in equation (2.9c) to zero and obtaining the free vibration response. It is this constraint normal mode that is used for the reduction of the system matrices. Considering equation (2.9c) and setting the boundary coordinates to zero, the remaining terms can be written as:

$$\underset{\sim}{A}^{II}\dot{\tilde{y}} + \underset{\sim}{B}^{II}\tilde{y} = \tilde{0} \tag{2.19}$$

Assuming the solution of the above equation in the form:

$$\tilde{y} = \tilde{y}_0 \, e^{\lambda t} \tag{2.20}$$

and substituting this into equation (2.19) and simplifying results in

$$\left(\lambda \, \underset{\sim}{A}^{II} + \underset{\sim}{B}^{II}\right)\tilde{y}_0 = \tilde{0} \tag{2.21}$$

or

$$\left(\left(\underset{\sim}{B}^{II}\right)^{-1}\underset{\sim}{A}^{II} + \frac{1}{\lambda}\underset{\sim}{I}\right)\tilde{y}_0 = \tilde{0} \tag{2.22}$$

or

$$\left(\underset{\sim}{D} - \hat{\alpha} \, \underset{\sim}{I}\right)\tilde{y}_0 = \tilde{0} \tag{2.23}$$

where

$$\underset{\sim}{D} = -\left(\underset{\sim}{B}^{II}\right)^{-1}\underset{\sim}{A}^{II} \tag{2.23a}$$

$$\hat{\alpha} = \frac{1}{\lambda} \tag{2.23b}$$

For nontrivial solution the coefficient of the determinate (2.23) must vanish, therefore:

$$|\underset{\sim}{D} - \hat{\alpha}\ \underset{\sim}{I}| = 0 \tag{2.24}$$

The solution of the above equation provides 2n eigenvalues λ_i and corresponding 2n displacement right eigenvectors $\tilde{U}_i$ where n is the number of component coordinates in second order form of equation (2.1). The 2n eigenvectors can be shown as:

$$\tilde{Y}_i = \begin{Bmatrix} \lambda_i \tilde{U}_i \\ \tilde{U}_i \end{Bmatrix} \quad \text{where} \quad i=1,\ldots 2n \tag{2.25}$$

or in matrix form as:

$$\underset{\sim}{Y} = \begin{bmatrix} \underset{\sim}{U}\underset{\sim}{\mathring{\Lambda}} \\ \underset{\sim}{U} \end{bmatrix} \tag{2.25a}$$

Therefore, the interior coordinates can be written in terms of these constrained normal modes of the above eigenvector expression so that:

$$\tilde{y}^I = \sum_{i=1}^{2n} \tilde{Y}_i \tilde{\eta}_i \tag{2.26}$$

or in matrix form

$$\tilde{y}^{I} = \begin{bmatrix} \underset{\sim}{U}\underset{\sim}{\mathring{\Lambda}} \\ \underset{\sim}{U} \end{bmatrix} \tilde{\eta} = \underset{\sim}{Y}\ \tilde{\eta} \tag{2.27}$$

where

$\underset{\sim}{Y}_{2n\times 2n}$ = matrix of constrained right vector

$\underset{\sim}{U}_{n\times 2n}$ = matrix of constrained right displacement U_i

$\mathring{\Lambda}_{2n\times 2n}$ = diagonal matrix of eigenvalues

$\tilde{\eta}_{2n\times 1}$ = vector of modal coordinates η associated with right vectors $\tilde{Y}_i$

2.3 Superposition of Component Modes

To obtain the complete modal transformation of the component physical coordinates, it is necessary to superpose the two modes, namely the constraint mode and the constrained normal mode, together to form a full modal transformation. From equation (2.27) the velocity constrained normal mode can be obtained so that:

$$\dot{\tilde{y}}^{I} = \underset{\sim}{Y}\ \dot{\tilde{\eta}} \tag{2.28}$$

and

$$\tilde{y} = \begin{Bmatrix} \tilde{y}^{B} \\ \tilde{y}^{I} \end{Bmatrix} = \begin{bmatrix} \underset{\sim}{I} & \underset{\sim}{0} \\ \underset{\sim}{0} & \underset{\sim}{Y} \end{bmatrix} \begin{Bmatrix} \tilde{y}^{B} \\ \tilde{\eta} \end{Bmatrix} \tag{2.29}$$

Therefore, the superposition of equations (2.29) and (2.18a) will give:

$$\tilde{y} = \begin{Bmatrix} \tilde{y}^B \\ \tilde{y}^I \end{Bmatrix} = \begin{bmatrix} \underset{\sim}{I} & \underset{\sim}{0} \\ \underset{\sim}{\Psi} & \underset{\sim}{Y} \end{bmatrix} \begin{Bmatrix} \tilde{y}^B \\ \tilde{\eta} \end{Bmatrix} \tag{2.30}$$

or

$$\tilde{y} = \underset{\sim}{\beta}\, \tilde{q} \tag{2.31}$$

where

$$\underset{\sim}{\beta} = \begin{bmatrix} \underset{\sim}{I} & \underset{\sim}{0} \\ \underset{\sim}{\Psi} & \underset{\sim}{Y} \end{bmatrix} \tag{2.31a}$$

2.3.1 Mode Truncation

The purpose of mode truncation is to eliminate the excessive unknown degrees of freedom, and hence to reduce the size of the system matrices without affecting the dynamic characteristics of the final system. Therefore all degrees of freedom of the system can be extensively reduced by retaining the low frequency mode and truncating a number of higher constrained normal modes determined from the free vibration analysis of interior coordinates. This can be considered as one of the most important aspects of the component mode synthesis technique. Based on the literature survey, researchers have not as of yet found any systematic way for mode truncation to guarantee convergence. One can, therefore, conclude that it is necessary to base mode truncation on prior experience.

At this stage, the entire degrees of freedom of the component can be reduced by eliminating the insignificant mode. Truncation can be established by partitioning $\underset{\sim}{Y}$ of constrained right vector and $\tilde{\eta}$ vector of modal coordinates in equation (2.27) such that:

$$\underset{\sim}{Y} = \left[\underset{\sim}{Y}_R \;\vdots\; \underset{\sim}{Y}_T \right] \tag{2.32}$$

and

$$\tilde{\eta} = \left\{ \begin{array}{c} \tilde{\eta}_R \\ \hline \tilde{\eta}_T \end{array} \right\} \tag{2.33}$$

Substituting the retained part of equation (2.32) and equation (2.33) into equation (2.30) results in the truncated modal transformation matrix β_R as shown below:

$$\tilde{y} = \begin{bmatrix} \underset{\sim}{I} & \underset{\sim}{0} \\ \underset{\sim}{\Psi} & \underset{\sim}{Y}_R \end{bmatrix} \left\{ \begin{array}{c} \tilde{y}^B \\ \tilde{\eta}_R \end{array} \right\} \tag{2.34}$$

or

$$\tilde{y} = \beta_R \, \tilde{q} \tag{2.35}$$

where

$$\beta_R = \begin{bmatrix} \underset{\sim}{I} & \underset{\sim}{0} \\ \underset{\sim}{\Psi} & \underset{\sim}{Y}_R \end{bmatrix} \tag{2.35a}$$

and

$$\tilde{q} = \begin{Bmatrix} \tilde{y}^B \\ \tilde{\eta}_R \end{Bmatrix} \qquad (2.35b)$$

The final truncated reduced component equation of motion is obtained by substituting equation (2.35) into equation (2.9d) and premultiplying by $\underset{\sim}{\beta}_R^T$ to obtain:

$$\underset{\sim}{\beta}_R{}^T \underset{\sim}{A} \underset{\sim}{\beta}_R \dot{\tilde{q}} + \underset{\sim}{\beta}_R{}^T \underset{\sim}{B} \underset{\sim}{\beta}_R \tilde{q} = \underset{\sim}{\beta}_R{}^T \tilde{Q} \qquad (2.36)$$

or

$$\bar{A}\, \dot{\tilde{q}} + \bar{B}\, \tilde{q} = \tilde{P} \qquad (2.37)$$

In order to assemble each truncated component with its adjacent component at interface, it is necessary to apply the $\underset{\sim}{k}$ transformation to the equation (2.37). This will assure connectivity between the two component coordinates. This transformation could have been avoided if proper care had been taken when constructing the modal transformation right vector (2.31a), since it would not have otherwise eased the computational efficiency. Therefore, the final $\underset{\sim}{k}$ reordering transformation to the truncated component is adopted such that:

$$\tilde{q} = \underset{\sim}{k}\, \tilde{q}_R \qquad (2.38)$$

substituting the above equation into equation (2.37) and premultiplying by $\underset{\sim}{k}^T$, the final reduced component can be written as:

$$\underset{\sim}{A}\,\dot{\tilde{q}}_R + \underset{\sim}{B}\,\tilde{q}_R = \tilde{P}_R \tag{2.39}$$

Finally the response of the system in generalized coordinates $\tilde{q}_R$ can be back transformed to obtain the relative physical coordinate through the transformation of equations (2.38), (2.35) and (2.8a), which combined together results in:

$$\tilde{h} = \begin{Bmatrix} \dot{\tilde{X}}_P^B \\ \dot{\tilde{X}}_P^I \\ \tilde{X}_P^B \\ \tilde{X}_P^I \end{Bmatrix} = \underset{\sim}{\bar{\alpha}}\,\beta_R \underset{\sim}{k}\,\tilde{q}_R \tag{2.40}$$

from the bottom half of equation (2.40) and (2.2a) the original coordinates $\tilde{X}^{(K)}$ can be determined.

2.4 System Equation of Motion

When all the components are analyzed by the aforementioned formulation and the truncated component equations are obtained, the truncated components are then assembled together to form the complete truncated system equation. If the system has only one component then the equation (2.39) will be the final system assembly. The next step is to include fluid film properties at bearing locations. The bearing has four degrees of freedom (two translations and two rotations) into which the fluid film damping and stiffness will be added the $\underset{\sim}{A}$ and $\underset{\sim}{B}$ of equation (2.39) respectively.

To incorporate pedestal into the system assembly, it is necessary to transform the pedestal properties into 2n form as cited earlier in equation (2.6), and then increase the size of the matrices of equation (2.39) (d.o.f of one pedestal in 2n form multiply by the number of pedestals) to accommodate the pedestal influence on the vibration response of the rotor.

To clarify how these properties are added into the assembly, a structure is considered to be composed of three components supported on two bearings as shown in Fig.2.4.1. The truncated components of the structure are obtained and assembled to form the three component assembly. The fluid film damping is added to the lower right quadrants of the two grids as shown in Fig.2.4.2, and the fluid film stiffness is added to the same location in Fig.2.4.3 The pedestal properties are then added to the assembly and the fluid film bearing is used as a connector between the pedestal and rotating assembly as clearly shown in Fig.2.4.2 and Fig.2.4.3.

To formulate the system assembly, assume κ to be the number of truncated components. The system coordinate vector

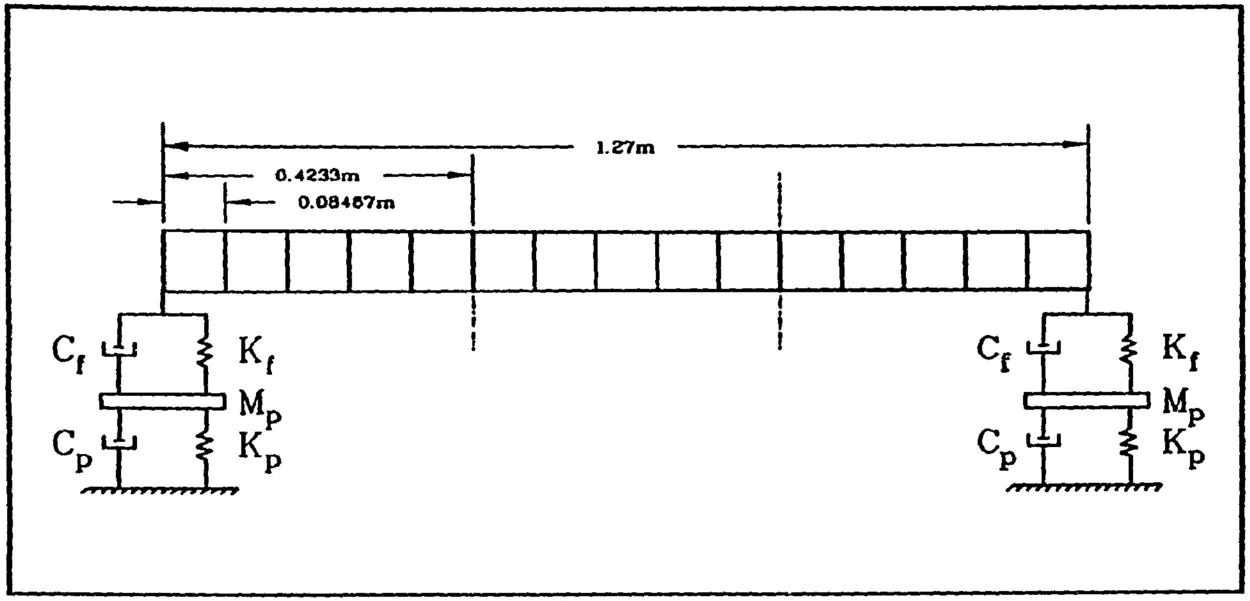

Fig.2.4.1 Rotor–bearing–pedestal system with three components. (only projection in Z–X plane is shown)

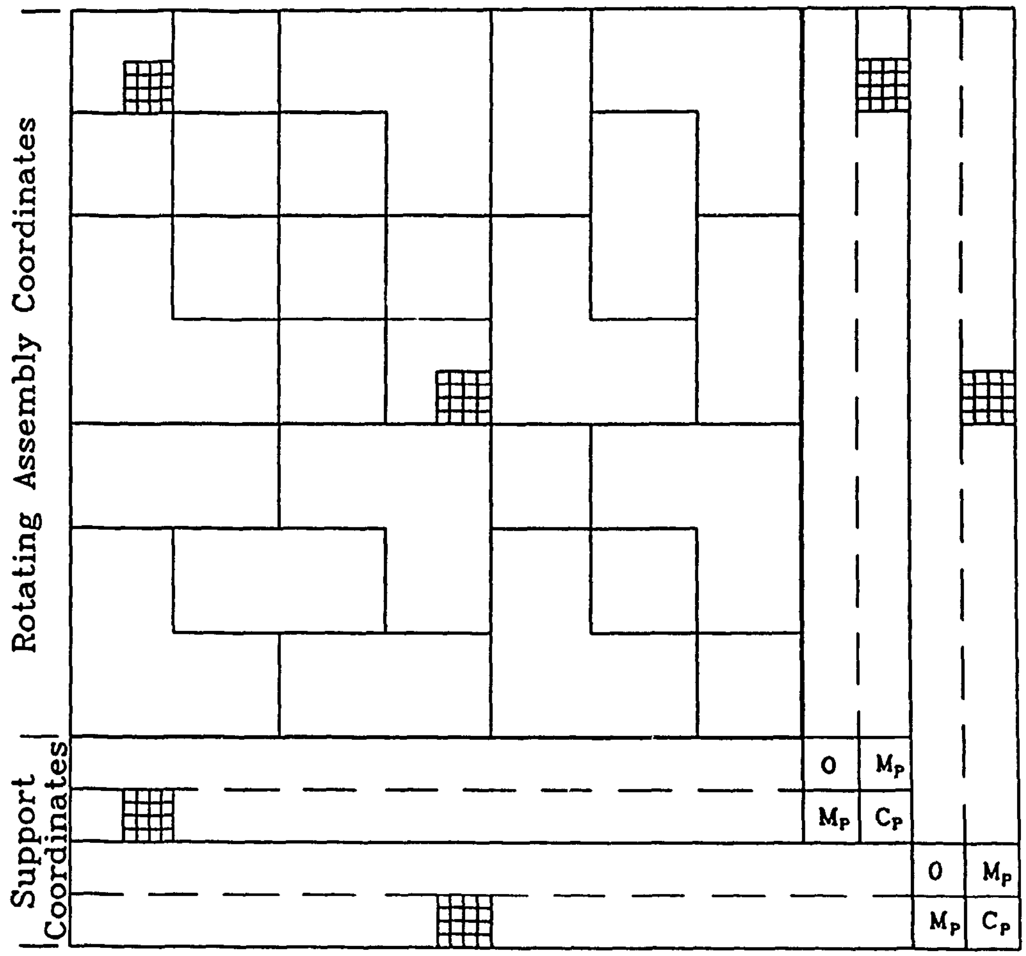

Fig. 2.4.2 Three component assembly matrix

Legend

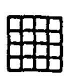
Bearing fluid film damping

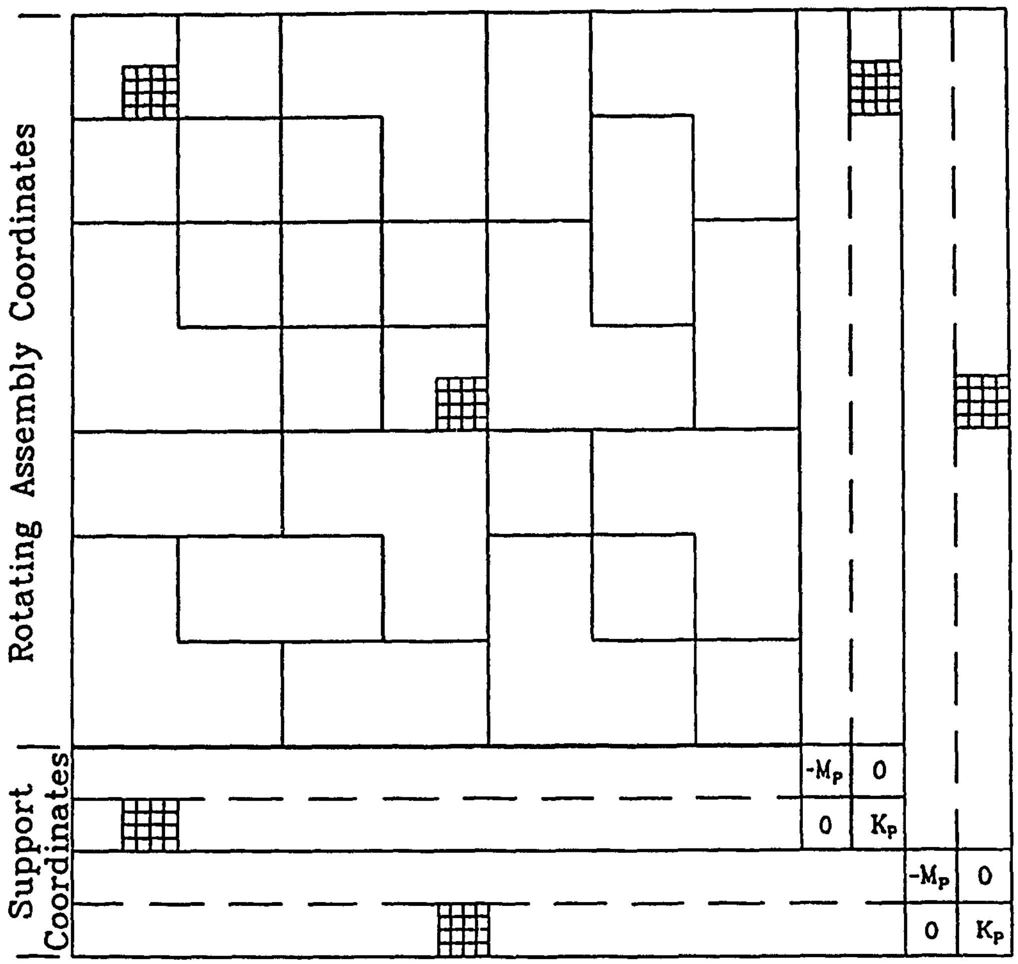

Fig. 2.4.3 Three component assembly matrix

Legend

Bearing fluid film stiffness

$\tilde{y}_s$ can be shown in terms of boundary and interior coordinates as:

$$\tilde{y}_S = \begin{Bmatrix} \tilde{y}_S^B \\ \tilde{\eta}_R^{(1)} \\ \tilde{\eta}_R^{(2)} \\ \vdots \\ \tilde{\eta}_R^{(K)} \end{Bmatrix} \tag{2.41}$$

The geometric constraint $\chi^{(K)}$ is then related to the component's coordinate vector to the system vector by the following expression:

$$\tilde{q}_R^{(K)} = \chi^{(K)} \tilde{y}_S \tag{2.42}$$

and by rewriting the equation (2.39) for kth component results in:

$$\mathcal{A}^{(K)} \dot{\tilde{q}}_R^{(K)} + \mathcal{B}^{(K)} \tilde{q}_R^{(K)} = \tilde{\mathcal{P}}_R^{(K)} \tag{2.43}$$

The system assembly can be obtained by substituting the transformation matrix of equation (2.42) into equation (2.43), premultiplying by $(\chi)^T$ and sum over all components. Hence:

$$\mathcal{A}_S \dot{\tilde{y}}_S + \mathcal{B}_S \tilde{y}_S = \tilde{\mathcal{P}}_S \tag{2.44}$$

$$\mathcal{A}_S = \sum_{K=1}^{N} (\chi^{(K)})^T \mathcal{A}_R^{(K)} \chi^{(K)} \tag{2.45a}$$

$$\underset{\sim}{\mathcal{B}}_S = \sum_{K=1}^{N} (\underset{\sim}{\chi}^{(K)})^T \underset{\sim}{\mathcal{B}}_R^{(K)} \underset{\sim}{\chi}^{(K)} \tag{2.45b}$$

$$\tilde{\mathcal{P}}_S = \sum_{K=1}^{N} (\underset{\sim}{\chi}^{(K)})^T \tilde{\mathcal{P}}_R^{(K)} \tag{2.45c}$$

where N is the number of components.

2.5 System Solution

The equation (2.44) can be decoupled by using the orthogonality property between normal modes if $\underset{\sim}{\mathcal{A}}_S$ and $\underset{\sim}{\mathcal{B}}_S$ were symmetric. Since $\underset{\sim}{\mathcal{A}}_S$ and $\underset{\sim}{\mathcal{B}}_S$ are not symmetric due to pedestal and bearing influence, decoupling the system equation of motion by conventional normal mode analysis is no longer possible. Therefore, it is necessary to use the biorthogonality principle between the right and the left eigenvectors of the system to decouple the system equations of motion. Right eigenvectors are the modes of the original system and the left eigenvectors are those of the transposed system. Right eigenvectors $\underset{\sim}{Y}$ are obtained by considering the free vibration of the system equation (2.44). The left eigenvectors are obtained by considering the free vibration of the transpose of system equation (2.44). To proceed by the above technique let the solution of equation (2.44) be of the form:

$$\tilde{Y}_S = \tilde{Y}_0 \, e^{\lambda_S t} \tag{2.46}$$

then

$$\left(\hat{\underset{\sim}{D}} - \hat{\alpha}_s \underset{\sim}{I} \; \tilde{y}_0\right) = \tilde{0} \tag{2.47}$$

and

$$\hat{\underset{\sim}{D}} = - \underset{\sim}{B}_s^{-1} \underset{\sim}{A}_s \tag{2.48a}$$

$$\hat{\alpha}_s = \frac{1}{\lambda_s} \tag{2.48b}$$

For nontrivial solution the determinant of equation (2.47) must vanish.

$$|\hat{\underset{\sim}{D}} - \hat{\alpha}_s \underset{\sim}{I}| = 0 \tag{2.49}$$

The solution of the above equation leads to j eigenvalues λ_s and j eigenvectors $\underset{\sim}{y}_s$, where j is the size of equation (2.44).

Left eigenvectors $\underset{\sim}{z}_s$ are obtained by solving the free vibration of the transposed equation (2.44) such that:

$$\tilde{z}_0^T \left(\lambda_s \underset{\sim}{A}_s + \underset{\sim}{B}_s\right) = \tilde{0}^T \tag{2.50}$$

This eigenvalue problem will result in identical j eigenvalues λ_s as in equation (2.44) and j left eigenvectors corresponding to each eigenvalue. Let us consider $\tilde{z}_0$ to be the left eigenvector of the following equation, therefore:

$$\tilde{z}_0^{\,T}\left(\underset{\sim}{\mathcal{A}}_s\underset{\sim}{\mathcal{B}}_s^{-1} + \frac{1}{\lambda}\underset{\sim}{I}\right) = \tilde{0}^T \tag{2.51}$$

For nontrivial solution the determinant of the above equation must vanish. Hence:

$$|\hat{\underset{\sim}{D}} - \hat{\alpha}_s\underset{\sim}{I}| = 0 \tag{2.52}$$

where

$$\hat{\underset{\sim}{D}} = -\underset{\sim}{\mathcal{A}}_s\,\underset{\sim}{\mathcal{B}}_s^{-1} \tag{2.53}$$

The left eigenvectors $\underset{\sim}{Z}_s$ resulting from equation (2.51) in matrix form and the right eigenvectors $\underset{\sim}{Y}_s$ resulting from equation (2.47) can be used to decouple the system equations of motion by considering the following transformation:

$$\tilde{Y}_s = \left[\underset{\sim}{Y}_s\right]\tilde{q} \tag{2.54}$$

substituting the above equation into equation (2.44) and premultiplying by $\underset{\sim}{Z}_s^{\,T}$ to obtain:

$$\underset{\sim}{Z}_s^{\,T}\underset{\sim}{\mathcal{A}}_s\underset{\sim}{Y}_s\dot{\tilde{q}} + \underset{\sim}{Z}_s^{\,T}\underset{\sim}{\mathcal{B}}\,\underset{\sim}{Y}_s\tilde{q} = \underset{\sim}{Z}_s^{\,T}\tilde{\mathcal{P}}_s \tag{2.55}$$

$$\left[\,\mathring{\underset{\sim}{N}}\,\right]\dot{\tilde{q}} + \left[\,\mathring{\underset{\sim}{M}}\,\right]\tilde{q} = \underset{\sim}{Z}_s^{\,T}\tilde{\mathcal{P}}_s \tag{2.56}$$

Then both sides of the equation are multiplied by the inverse of $\mathring{\underset{\sim}{N}}$ which results in the final system equation of motion.

$$\dot{\tilde{q}} = -\mathring{\underset{\sim}{\Lambda}}_s\tilde{q} + \tilde{\zeta} \tag{2.57}$$

where

$$\tilde{\zeta} = \mathring{\underset{\sim}{N}}\ \underset{\sim}{Z}_s{}^T \tilde{\mathcal{P}}_s \tag{2.58}$$

Any prescribed ground motion can now be applied to the system and the result can be back transformed to the original coordinates.

CHAPTER 3

COMPUTER IMPLEMENTATION

3.1 Introduction

A computer program has been developed to perform the analysis by the component mode synthesis method described in chapter 2. This program can handle any number of bearings, and pedestal, and their flexibilities. It can yield natural frequencies and critical speeds as well as the response against any prescribed forced excitation.

3.2 Description of Computer Program SETSA

3.2.1 General

Free vibration response of rotor-bearing-pedestal system is analyzed by the computer program **SETSA**. The program is written in FORTRAN Language. It is based on the finite element method which can handle rotor-bearing system analysis in the linearly elastic range.

The computer program **SETSA** is specifically organized to handle the response of the system by component mode synthesis technique based on the formulation described in chapter 2. The response of the system is obtained by numerically integrating a set of generalized decoupled system equations of motion. It is also possible to obtain the response of the system by finite element method alone provided that the size of the matrices does not exceed the computer capacity and other resource limitations. The program will bypass finite element technique unless it is specified.

Since the formulation of system motion (chapter 2) is based on fixed reference frame to describe the system motion; nonsymmetric support characteristics such as damping and stiffness can, therefore, be easily accommodated by the program.

The rotating assembly may contain up to four components each of which may be composed of several finite elements of different length and diameter; this will, therefore, allow reasonable flexibility in modeling the system with several geometric discontinuities. The bearing-pedestal is considered to be fixed in a rigid frame foundation whose translational and rotational motion may be specified by the user.

3.2.2 Sequence of Computation

The steps involved in the calculations performed by the computer program SETSA are as follows:

1. The program accepts the user input data such as

element diameter, length, modulus of elasticity, density, mass, stiffness and possibly structural damping of element and prepares the output to verify the input data.

2. Analyzes the internal precessional mode of each component. Output includes the internal damping or undamped whirl mode and frequencies. This will help the user to obtain more information about each component as well as the number of mode truncation. The optional plotting of these modes can also be obtained.

3. Provides the steady state and transient response of the rotating assembly relative to the rigid base due to the specified base motion (e.g. sinusoidal and impulsive) with constant spin speed restriction. The output contains the displacements and rotations at each finite element station.

3.3 Flow Charts and Subroutine Descriptions

The flow charts for the computer program SETSA are shown in Appendix A and the description of the sub-programs used are outlined below:

3.3.1 Program MAIN

This program will execute the sub-programs in a sequential order and the important information will be recorded on different TAPE. For example the output of the first sub-program will be inputted to the second subprogram and so on. It will always record the important information such as eigenvalues and eigenvectors of each component and also the system assembly in damped and undamped situation. Finally the program MAIN will record the response of the system subjected to any base sinusoidal excitation although it is not pursued in this investigation.

3.3.2 Sub-Program CMS1

This sub-program prepares the element mass, stiffness and damping matrices from the input data, and assembles the number of elements to determine the component mass, stiffness and damping matrices. The component stiffness matrix is then recorded on the output unit TAPE4. The component matrices will then be reordered to first order form component equations of motion. The first order matrices are recorded on the output unit TAPE1 and TAPE2. Finally, the transformation matrix which can reorder the first order form into boundary and interior subset is developed and recorded on TAPE3.

Called Subroutines: BUILD, ASSEMBLY

3.3.3 Sub-Program CMS2

This program will read TAPE1,2,3,4, and obtain the static mode as shown in equation (2.13) and record the transformation matrix $[\psi]$ on TAPE9 as indicated in equation (2.13a) and also record the matrices of the interior coordinates on TAPE21 and TAPE22.

Called Subroutine: (IMSL Subroutine - DLINRG)

3.3.4 Sub-Program CMS3

This subroutine will read the interior coordinates from TAPE21 and TAPE22 to determine the rotating assembly component precessional mode with fixed boundary coordinates. The precessional mode and frequency are then recorded on TAPE17 and TAPE10 respectively. It is in this subroutine that interior truncation is performed.

Called Subroutine: ARRANG, CMPOS, (IMSL Subroutine - E2CCG, LINCG)

3.3.5 Sub-Program CMS4

This subroutine will read TAPE7,9,11,12,17 to determine the transformation matrix by superposing the static and truncated dynamic mode. This transformation is then recorded on TAPE15. Using the above transformation matrix to component equation, the reduced component matrices can then be obtained. The reduced component equation is recorded on TAPE41,42.

Call Subroutine: None

3.3.6 Sub-Program CMS5

This subroutine will read TAPE3, 15, 19 to perform back transformation of truncated reduced component to original coordinates and record the back transformation matrix on TAPE45. Thus it is concluded that for one component assembly TAPE41, 42, 45 are the most important records needed to proceed further. For two, three, and four component assembly the sub-program CMS1, CMS2, CMS3, CMS4 and CMS5 will repeat 2, 3, and 4 times and record the important information on TAPE41, 42, 45, TAPE51, 52, 55, TAPE61, 62, 65 and TAPE71, 72, 75.

Called Subroutine: None

3.3.7 Sub-Program CMSASS

This subroutine will read the information for each component, for example TAPE41,42, TAPE51,52, TAPE61,62, and TAPE71,72. Then assemble them in such a way as shown in Fig.2.4.2 and Fig.2.4.3. The assembled matrices are recorded on TAPE23,24. The fluid film and pedestal properties are then added to the system and the results of matrices are recorded on TAPE25,26 for further analysis of the system reponse.

Called Subroutine: None

3.3.8 Sub-Program CMSUND

This subroutine will analyze the undamped response of the assembly by reading the information of the component assembly matrices from TAPE23,24 and calculate the undamped natural frequencies and mode shape of the system and record them on TAPE10 and TAPE66 respectively.
Called Subroutine: ARRANG, CMPOS, ELIM, (IMSL subroutine-E2CCG, L2NCG)

3.3.9 Sub-Program CMSDAM

The sub-program CMSDAM will read TAPE25 and TAPE26 component assembly matrices to obtain the left and right eigenvectors by calling the IMSL [38] routine, then by using biorthogonality relation will decouple the equation of motion. Here TAPE10 will record the diagonal eigenvalue of damped system and TAPE200 will have the forcing coefficient matrix.
Called Subroutine: ARRANG, CMPOS (IMSL subroutine-E2CCG, L2NCG)

3.3.10 Sub-Program CMSRES

This program will read TAPE10, and TAPE200 with specified time step to calculate the response of the system in local coordinates. Then by back transformation matrices which are provided by reading from TAPE45,55,65, and TAPE75 will transform to original coordinates. The modal response of the system is recorded on TAPE400. The plotting of response is then possible. Since the forcing response is not included in the present analysis, therefore, the flow chart of the sub-program CMSRES is not included in Appendix A.

Called Subroutine: None

3.4 Validation of the Program

3.4.1 General

The computer program based on mathematical development in chapter 2 is tested with the use of two detailed examples in the following section to provide a clear insight into the accuracy and limitations of the method. In the following examples the natural frequency of the rotor is calculated and the variation of error against different levels of truncation is described.

3.5 Example Analysis

3.5.1 Rotor System 1

i) The first example discussed here is a simply supported Lund [39] rotor shown in Fig.3.5.1a. First the entire rotor is considered as a single component. The rotor

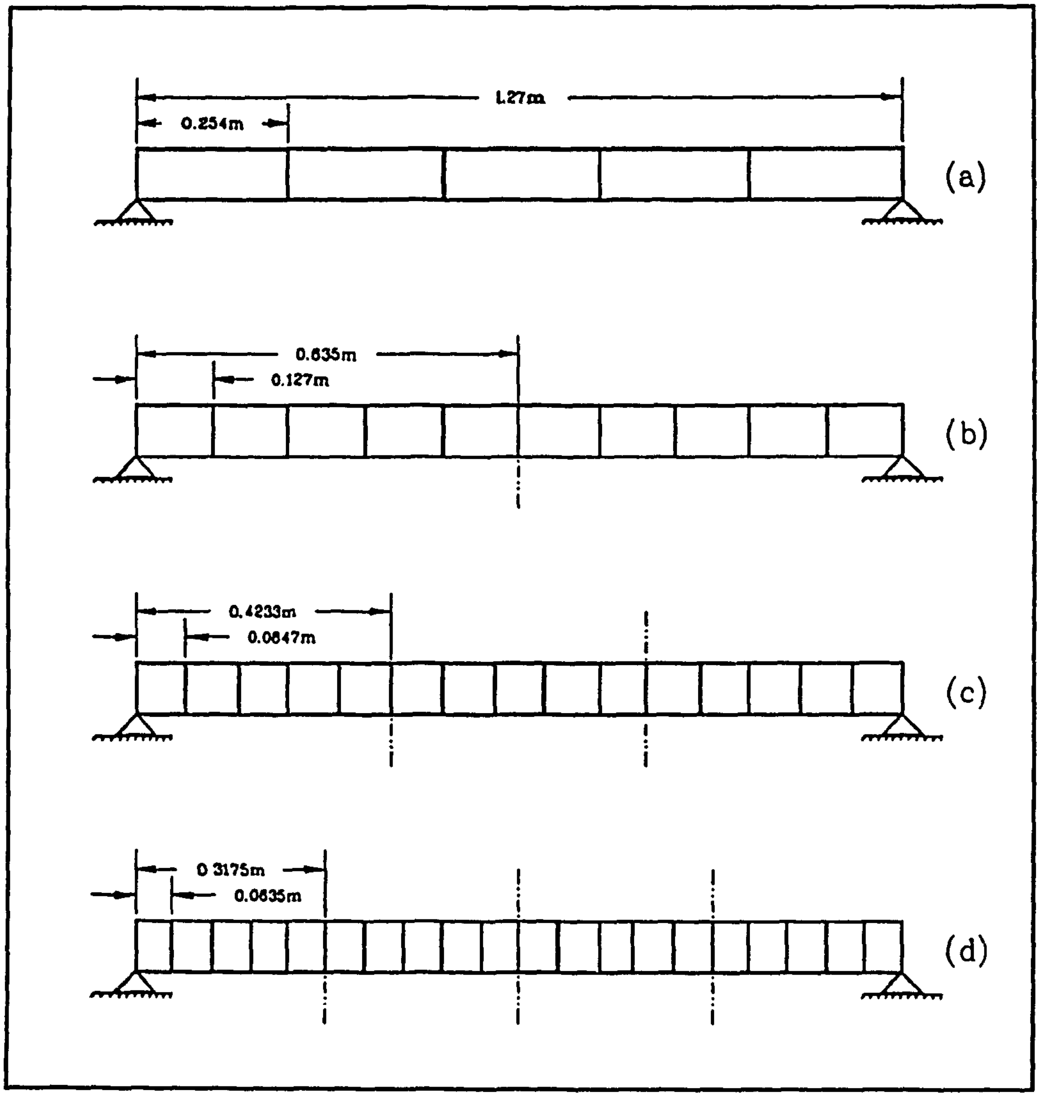

Fig.3.5.1 Simply supported undamped Lund rotor composed of: a) one component, b) two component, c) three component and d) four component assembly.

is modeled with 5 equal length finite elements (6 stations) each with four degrees of freedom per station. The degrees of freedom in each station are represented by two translations and two rotations in Z and Y direction. The total number of degrees of freedom is 24 or (N+1)*4 where N is the number of elements.

The rotor supports at station 1 and 6 are assumed to be rigid and unyielding against translational displacements; however, rotation about the two bending axes is permitted. Damping at the bearing is neglected. The rotor, therefore, has four constraint modes which are identical to rigid body modes and the rotating assembly contains 20 degrees of freedom (total degrees of freedom minus number of constraints). The rotor is modeled symmetric about its mass center. The natural frequencies of the system are obtained by eliminating the rows and columns of those coordinates associated with translation in support points. The result is tabulated for different levels of mode truncation as shown in Table 3.1.

ii) The rotor is considered to be composed of two components, as shown in Fig.3.5.1b, each component contains five equal length finite elements. First, each component will be analyzed separately, and the size of the component will be reduced for different levels of mode truncation. The truncated reduced components are assembled to form the system assembly. The tabulated results for different levels

Table 3.1

Natural Frequencies of One Component Assembly at Different Levels of Mode Truncation					
No.	Retain 4 Mode	Retain 8 Mode	Retain 12 Mode	Retain 20 Mode	Retain All Mode
1	126.864	126.864	126.855	126.855	126.855
2	641.096	505.186	505.186	504.849	504.835
3	1546.611	1546.615	1130.324	1128.645	1128.521
4	--------	2850.855	2850.855	1999.210	1995.453
5	--------	--------	4525.956	3119.284	3111.106
6	--------	--------	--------	6517.288	4748.115
7	--------	--------	--------	8073.554	6279.373
8	--------	--------	--------	--------	8410.807
9	--------	--------	--------	--------	11030.337
10	--------	-------	--------	--------	14091.646

Lund rotor

of mode truncation are shown in Table 3.2. The accuracy of the results monotonically decrease by increasing the levels of mode truncation.

iii) This time the rotor is divided into three and finally four components Fig.3.5.1c, and Fig.3.5.1d. The same procedure is adopted as in part (i) and (ii), and the result of the assembly for different levels of mode truncation is shown in Tables 3.3 and 3.4. The results obtained here are similar to those observed in Table 3.2; however, it is more accurate due to the increase in the number of components, which in turn depend on the number of elements used.

3.5.2 Rotor System 2

The second example presented here is a typical overhung industrial rotor. The rotor is divided into four components wherein each component consists of several disks, couplings and bearings. The rotor is also supported by two identical bearings as shown in Fig.3.5.2 and it possesses four degrees of freedom per node (two translations and two rotations) in Z and Y direction. The number of constraint degrees of freedom is four (two constraints degrees of freedom per support), the rotor support is assumed to be undamped with infinite stiffness properties. The total number of degrees of freedom precessional mode is (N+1)*4 minus constraint degrees of freedom. The numerical data for this rotor is

Table 3.2

Natural Frequencies of Two Component Assembly at Different Levels of Mode Truncation					
No.	Retain 4 Mode	Retain 8 Mode	Retain 12 Mode	Retain 20 Mode	Retain All Mode
1	126.860	126.852	126.8497	126.849	126.849
2	504.525	504.525	504.4824	504.481	504.481
3	1156.426	1125.603	1125.2418	1124.732	1124.692
4	2503.101	1977.040	1977.0402	1975.581	1975.504
5	4112.930	3166.255	3046.9970	3043.671	3043.305
6	5851.553	5851.553	4321.1765	4315.612	4315.145
7	----	8104.688	6013.3910	5789.229	5780.586
8	----	10356.494	10356.494	7448.477	7431.932
9	----	----	13073.519	9267.640	9254.835
10	----	----	15687.175	11962.114	11922.512

Lund rotor

Table 3.3

Natural Frequencies of Three Component Assembly at Different Levels of Mode Truncation					
No.	Retain 4 Mode	Retain 8 Mode	Retain 12 Mode	Retain 20 Mode	Retain All Mode
1	126.850	126.849	126.848	126.848	Size of matrices exceeded the computer capacity
2	504.645	504.468	504.445	504.438	
3	1124.335	1124.335	1124.216	1124.212	
4	2004.106	1973.675	1973.641	1972.966	
5	3169.379	3039.555	3036.034	3034.020	
6	5422.612	4292.800	4292.800	4288.749	
7	7280.533	5861.691	5722.816	5718.428	
8	--------	7697.238	7320.881	7305.872	
9	--------	--------	9047.626	9032.991	
10	--------	--------	--------	12881.762	

Lund rotor

Table 3.4

Natural Frequencies of Four Component Assembly at Different Levels of Mode Truncation					
No.	Retain 4 Mode	Retain 8 Mode	Retain 12 Mode	Retain 20 Mode	Retain All Mode
1	126.848	126.848	126.848	Size of matrices exceeded the computer capacity	Size of matrices exceeded the computer capacity
2	504.477	504.444	504.432		
3	1125.007	1124.240	1124.166		
4	1972.734	1972.734	1972.465		
5	3066.721	3033.196	3033.188		
6	4402.052	4287.346	4286.428		
7	6007.132	5721.932	5711.647		
8	9182.582	7289.425	7289.425		
9	--------	9153.271	8993.439		
10	--------	11198.397	10817.150		

Lund rotor

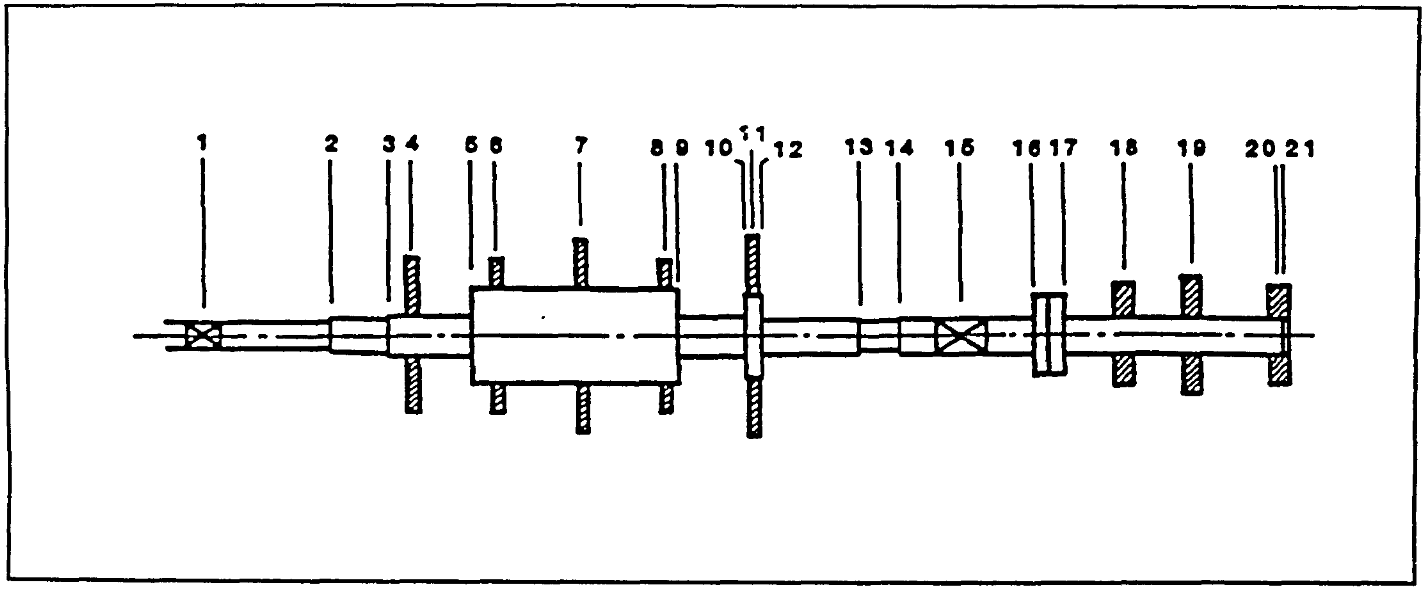

Fig.3 5 2 Prohl rotor [2]

$E = 2.068E11$ N/m^2

$\rho = 7800$ Kg/m^3

taken from reference [2]. The natural frequency of the system assembly is tabulated for different levels of mode truncation which is shown in Table 3.5.

3.6 Discussion of Results

It can be seen from the results presented in Table 3.6, Fig.3.6.1 and Fig.3.6.2 that the accuracy monotonically increases with the increase in the number of components chosen for analysis. When a fewer number of components and/or elements are utilized, only the higher mode frequency is affected more by the truncations. However, the lower mode frequencies are not significantly affected by truncation. The calculated result obtained by this method is in accord with those achieved by Lund [39] and by Prohl [2]. The accuracy of the method and the computer program SETSA is thus established.

Table 3.5

Natural Frequencies of Four Component Assembly at Different Levels of Mode Truncation					
No.	Retain 4 Mode	Retain 8 Mode	Retain 12 Mode	Retain 20 Mode	Retain All Mode
1	2158.956	2158.869	2158.820	2158.820	Size of matrices exceeded the computer capacity
2	4235.044	4234.570	4234.205	4234.203	
3	11130.943	11108.881	11106.726	11106.679	
4	21387.542	21367.080	21363.811	21361.816	
5	27390.719	27380.412	27379.491	27378.579	
6	36980.788	36873.249	36831.039	36830.644	
7	68122.308	57825.075	57235.564	57137.098	

Prohl rotor

Table 3.6

Error at Different Levels of Mode Truncation				
No.	% Error 4 Mode Retain	% Error 8 Mode Retain	% Error 12 Mode Retain	% Error 20 Mode Retain
1	0.00939	0.00282	0.000938	0.000638
2	0.01836	0.01836	0.009805	0.009610
3	2.86960	0.1278	0.0956	0.05035
4	26.9020	0.2319	0.2319	0.15795
5	35.597	4.386	0.4550	0.3455
6	36.51	36.517	0.8106	0.6807

Lund rotor

Fig.3.6.1 Influence of Mode Truncation on N.F of the Rotor

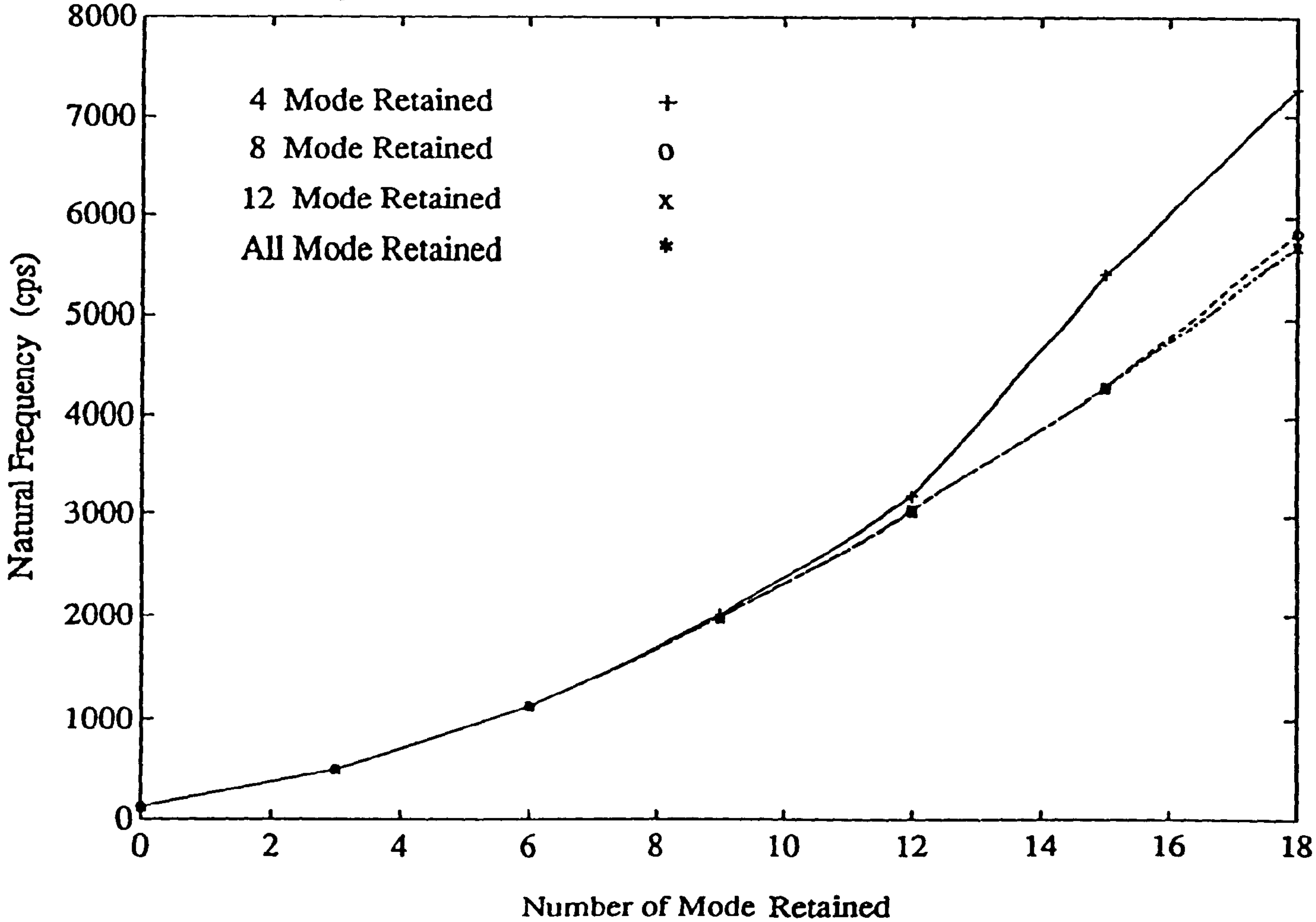

Fig.3.6.2 Error at Different Level of Mode Truncation

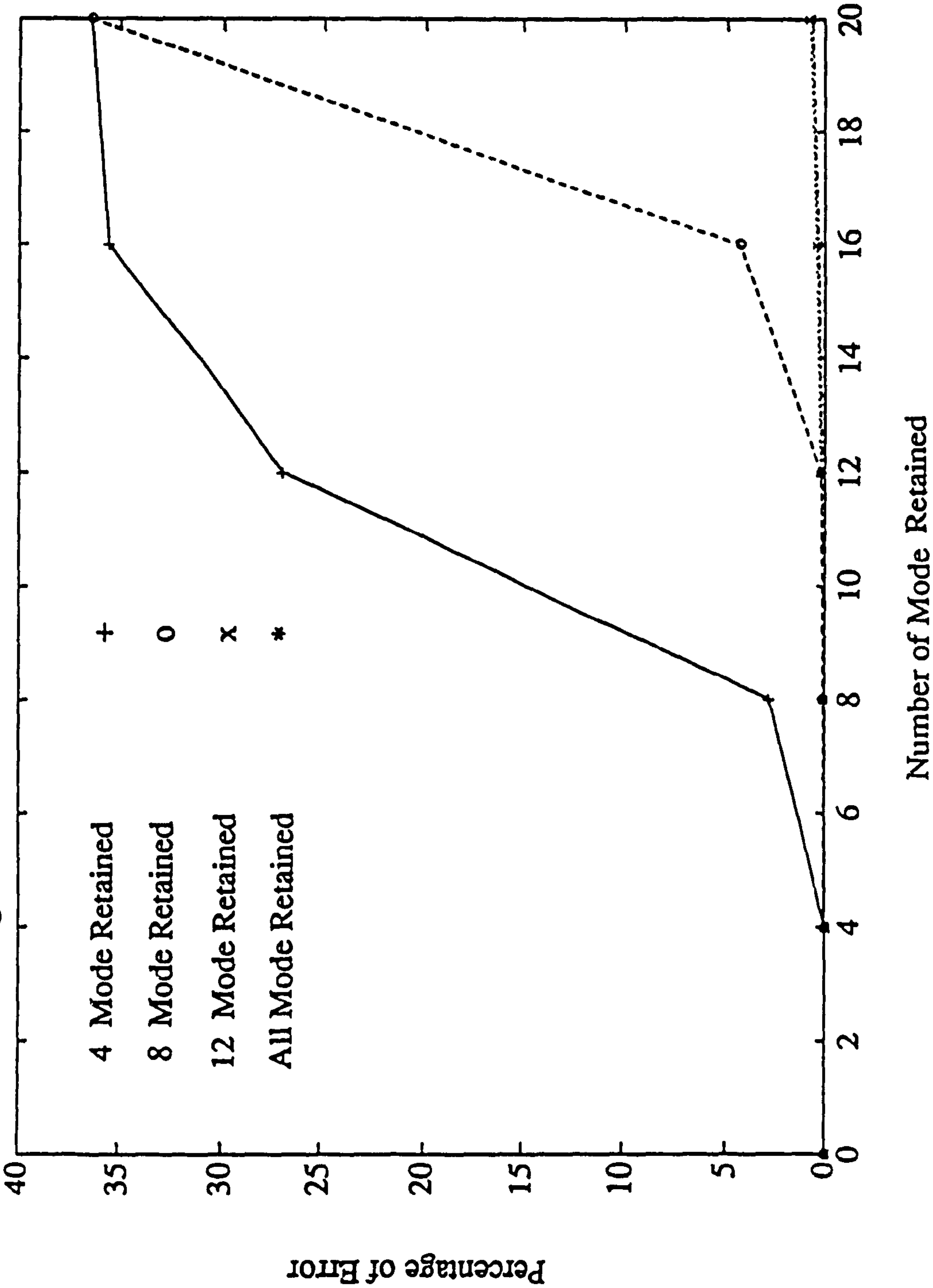

CHAPTER 4

PARAMETRIC STUDY OF ROTOR-BEARING-PEDESTAL SYSTEM

4.1 Introduction

In chapters 2 and 3, a component mode synthesis reduction method based on biorthogonality relation is formulated and adopted to decouple the system equation of motion. Based on this formulation the computer program **SETSA** is developed in chapter 3 to obtain the response of the system. In this chapter the computer program **SETSA** is used to perform a detailed parametric study on a single disk rotor-bearing-pedestal system mounted on flexible support. Even though the analysis procedure discussed here is confined to a single disk rotor system model which can be well represented by a few finite elements, the same treatment is equally applicable for a large practical rotor system with several disks, couplings and bearings.

A typical flexible rotor-bearing-pedestal system in a deformed state is shown in Fig.2.2.1. The rotor is composed of symmetrical rotor segments with distributed mass and elasticity properties, a symmetric rigid disk and the two bearings situated at each end of the rotor. The rotor of Noriaki et al [40] is chosen for the study here. The Noriaki rotor configuration with a single disk mounted at three different locations is illustrated in Fig.4.1.1.

The influence of the following parameters on the critical speed of the rotor is investigated:

1. Rotor Stiffness Parameter EI/ℓ^3
2. Rotor Material Density
3. Disk Thickness and Disk Location
4. Support Stiffness
5. Support Damping
6. Pedestal Mass

4.2 Influence of Rotor Stiffness parameter EI/ℓ^3 on Critical Speed of the Rotor

The computations are performed for different values of the rotor stiffness parameter EI/ℓ^3 (Appendex B) ranging from 57×10^5 to 162×10^5 N/m in steps of 175×10^3 N/m. The single disk rotor for this study consists of six equal length finite elements. The disk position and disk thickness remain constant throughout the analysis (ℓ_1 = 0.533m and ℓ_2 = 0.266m) as shown in Fig.4.2.1b and 4.1.1b. The response of the system is obtained for two different rotor configurations: namely, a) simply supported on rigid supports (undamped) and b) simply supported on hydrodynamic journal bearing (damped). In the case of the undamped rotor, the stiffness and damping of fluid film and pedestal properties

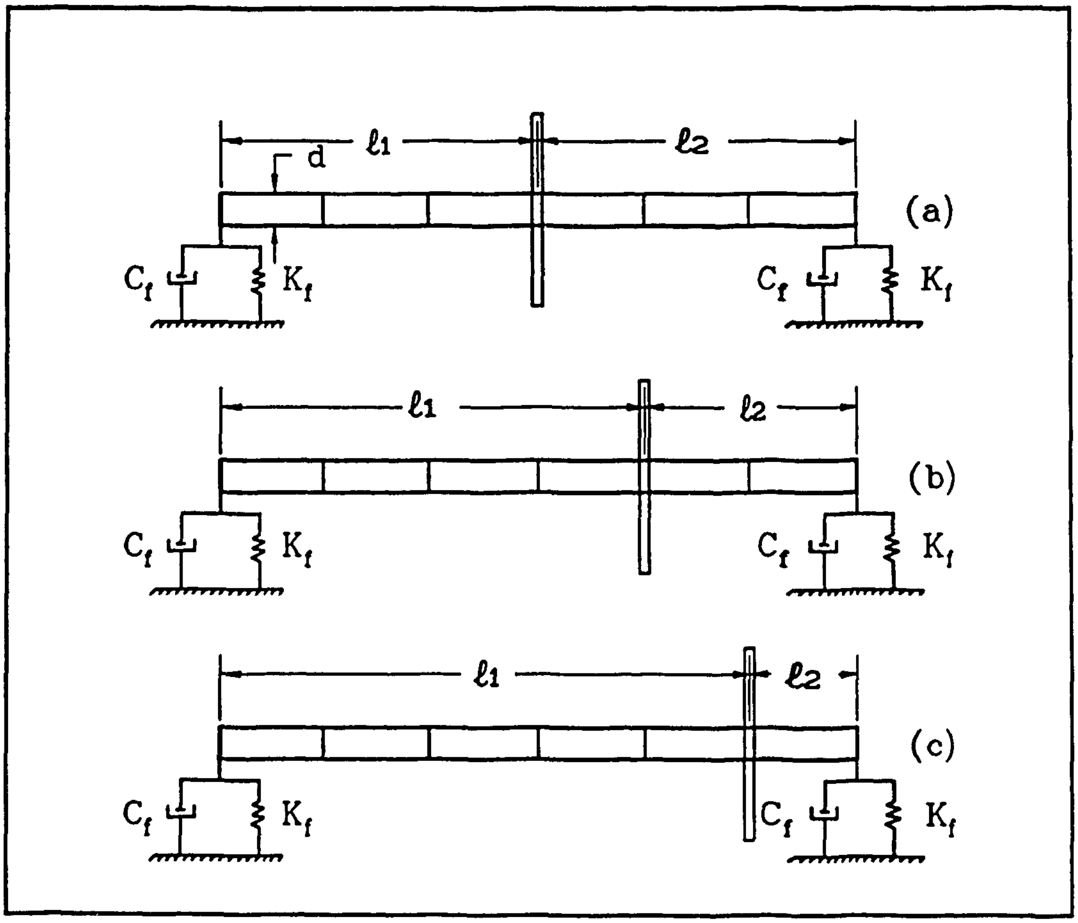

Fig.4.1.1 Simply supported damped rotor with a single disk mounted at three different locations

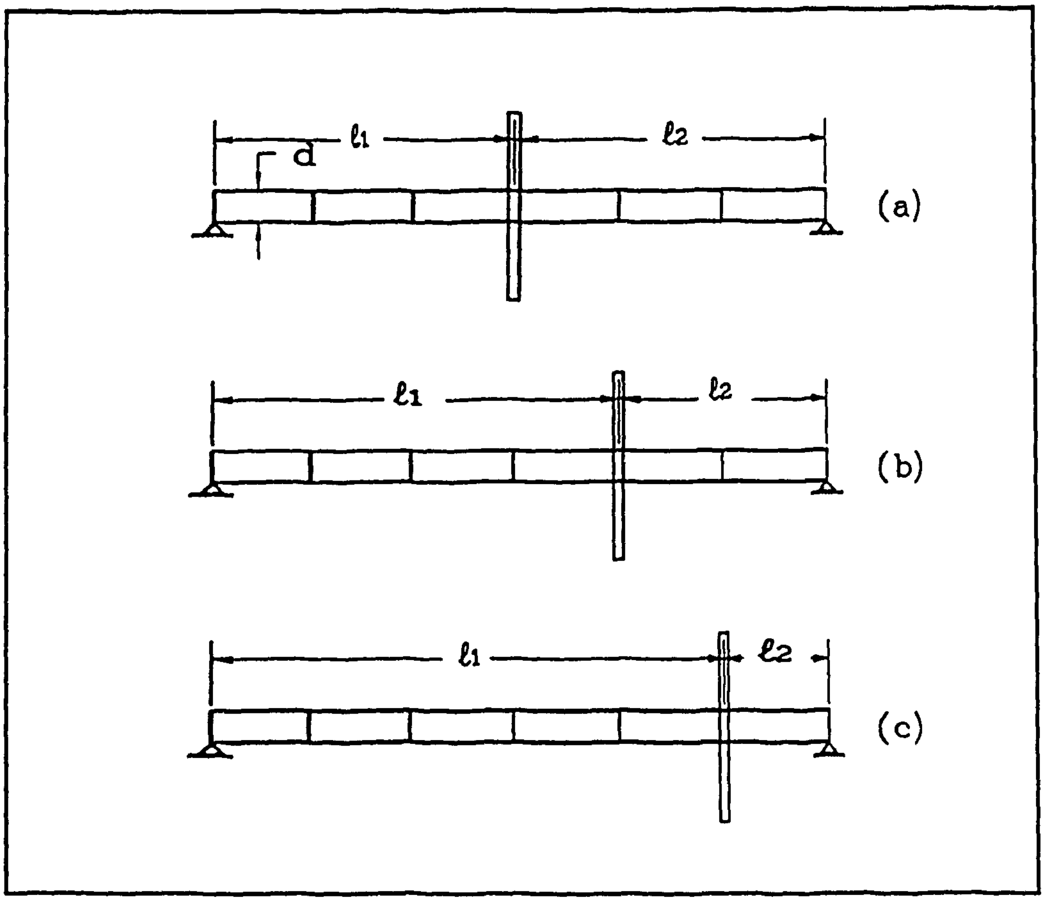

Fig. 4.2.1 Simply supported undamped rotor with a single disk mounted at three different locations

are neglected; whereas, in the damped rotor these properties are all lumped together. In both cases the pedestal mass is neglected and the same levels of mode truncations are employed. In each case the resonance frequency of the first four modes are obtained and presented in Tables 4.2.1 and 4.2.2. A plot of the critical speed vs the rotor stiffness parameter is shown in Fig.4.2.2.

It is clear from the result obtained for both the damped and undamped situation, that as the stiffness parameter EI/ℓ^3 is increased the natural frequency of the system also increases monotonically. This behavior is more pronounced in the undamped configuration in that the natural frequency of the undamped response for a particular stiffness parameter is higher than in the damped rotor.It is, therefore, possible to control the response of a system by changing the stiffness parameter of the rotor.

4.3 Influence of Rotor Material Density on Critical Speed of the Rotor

The computer simulation is performed for the different material densities of the rotor. The rotor material densities are listed in Table 4.3.1. The rotor is assumed to be simply supported with a disk mounted on its mid-section ($\ell_1 = \ell_2 = 0.4m$). It is composed of six finite beam elements. The thickness of the disk remains constant

Table 4.2.1

Influence of (EI/ℓ^3) Coefficient on the Undamped Critical Speed of the Rotor					
No.	Mode 1 (CPS)	Mode 2 (CPS)	Mode 3 (CPS)	Mode 4 (cps)	EI/ℓ^3 (N/m)
1	69.0795	254.078	425.7783	1095.084	57.13E5
2	78.9625	290.428	486.6935	1251.755	74.65E5
3	87.7393	322.709	540.7900	1390.889	92.16E5
4	95.7146	352.043	589.9467	1517.318	109.67E5
5	103.0747	379.114	635.3113	1633.994	127.18E5
6	109.9431	404.376	677.6458	1742.876	144.69E5

$E = 2.068E11$ N/m^2

$\rho = 7800$ Kg/m^3

$\ell_1 = 0.533$ m

$\ell_2 = 0.266$ m

Table 4.2.2

Influence of (EI/ℓ^3) Coefficient on the damped Critical Speed of the Rotor					
No.	Mode 1 (CPS)	Mode 2 (CPS)	Mode 3 (CPS)	Mode 4 (CPS)	EI/ℓ^3 (N/m)
1	48.7634	113.9670	212.8807	439.8154	57.13E5
2	51.6954	116.0418	231.1330	499.6345	74.65E5
3	53.7704	117.3581	247.9575	553.2198	92.16E5
4	55.3151	118.2669	263.6902	602.1415	109.67E5
5	56.5089	118.9317	271.5780	647.4210	127.18E5
6	57.4587	119.4390	285.7341	689.7594	144.69E5
7	58.2320	119.8388	299.2854	729.6606	162.2E5

$E = 2.068E11$ N/m^2

$\rho = 7800$ Kg/m^3

$\ell_1 = 0.533$ m

$\ell_2 = 0.266$ m

Kzz = 981E3 N/m

Kyy = 981E3 N/m

Czz = 981 N-sec/m

Cyy = 981 N-sec/m

Fig.4.2.2 Influence of Stiffness Parameter EI/L**3 on N.F of the Rotor

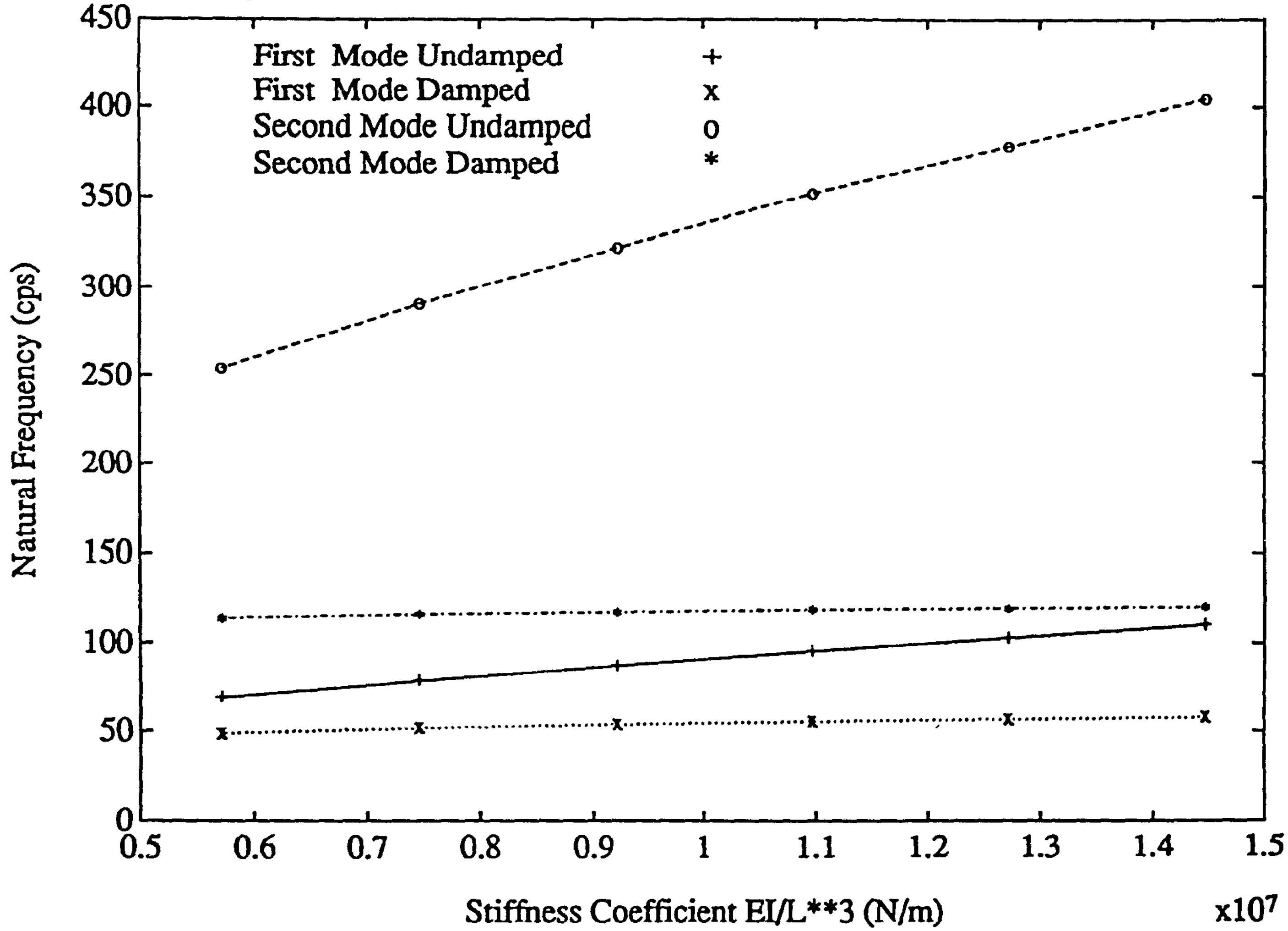

Table 4.3.1

Material Properties of the Rotor		
Material	Density kg/m^3	Modulus of E N/m^2
Cast Iron	7200	2.068×10^6
Stainless Steel (430)	7700	2.068×10^6
Steel (4150)	7800	2.068×10^6
Stainless Steel (302)	7900	2.068×10^6
Cobalt	8850	2.068×10^6
Nickel	8900	2.068×10^6

throughout the simulation and is assumed to be 0.01 m. The rotor configuration is shown in Fig.4.2.1a. The results are obtained by varying the density of the rotor from 7200 to 8900 kg/m^3. Tne selected materials have the same modulus of elasticity of 2.068x10^{11} N/m^2. The results of the simulations are then tabulated in increasing order of frequency as shown in Table 4.3.2. Finally a plot of the response vs the different material densities of the rotor is shown in Fig.4.3.1.

Material density of the rotor also influences the response of the system. As the material density increases the rotor critical speed decreases. The decreasing rate is more rapid in the higher mode. It is also observed that the third and forth mode behave almost identically throughout the density range. It is, therefore, important to consider material density in the dynamic analysis of the rotor bearing system.

4.4 Influence of Disk Thickness and Disk Location on Critical Speed of the Rotor

The result of the computer simulation is obtained for the different values of disk thickness and disk location. The rotor is assumed to be simply supported and consists of six equal distance finite elements with a disk located on three different locations ($\ell_1 = \ell_2 = 0.4$m, $\ell_1 = 0.533$m and

Table 4.3.2

Influence of Material Density on the Undamped Critical Speed of the Rotor					
No.	Mode 1 (CPS)	Mode 2 (CPS)	Mode 3 (CPS)	Mode 4 (cps)	Density μ (Kg/m^3)
1	95.87	339.18	963.03	966.33	7200
2	92.7	327.9	931.24	934.40	7700
3	92.1	325.86	925.22	928.5	7800
4	91.52	323.8	919.38	922.5	7900
5	86.47	305.92	868.59	871.56	8850
6	86.23	305.07	866.18	869.15	8900

$E = 2.068E11$ N/m^2

$\rho = 7800$ Kg/m^3

$\ell_1 = 0.4$ m

$\ell_2 = 0.4$ m

$t_d = 0.01$ m

Fig.4.3.1 Influence of Material Density on N.F of the Rotor

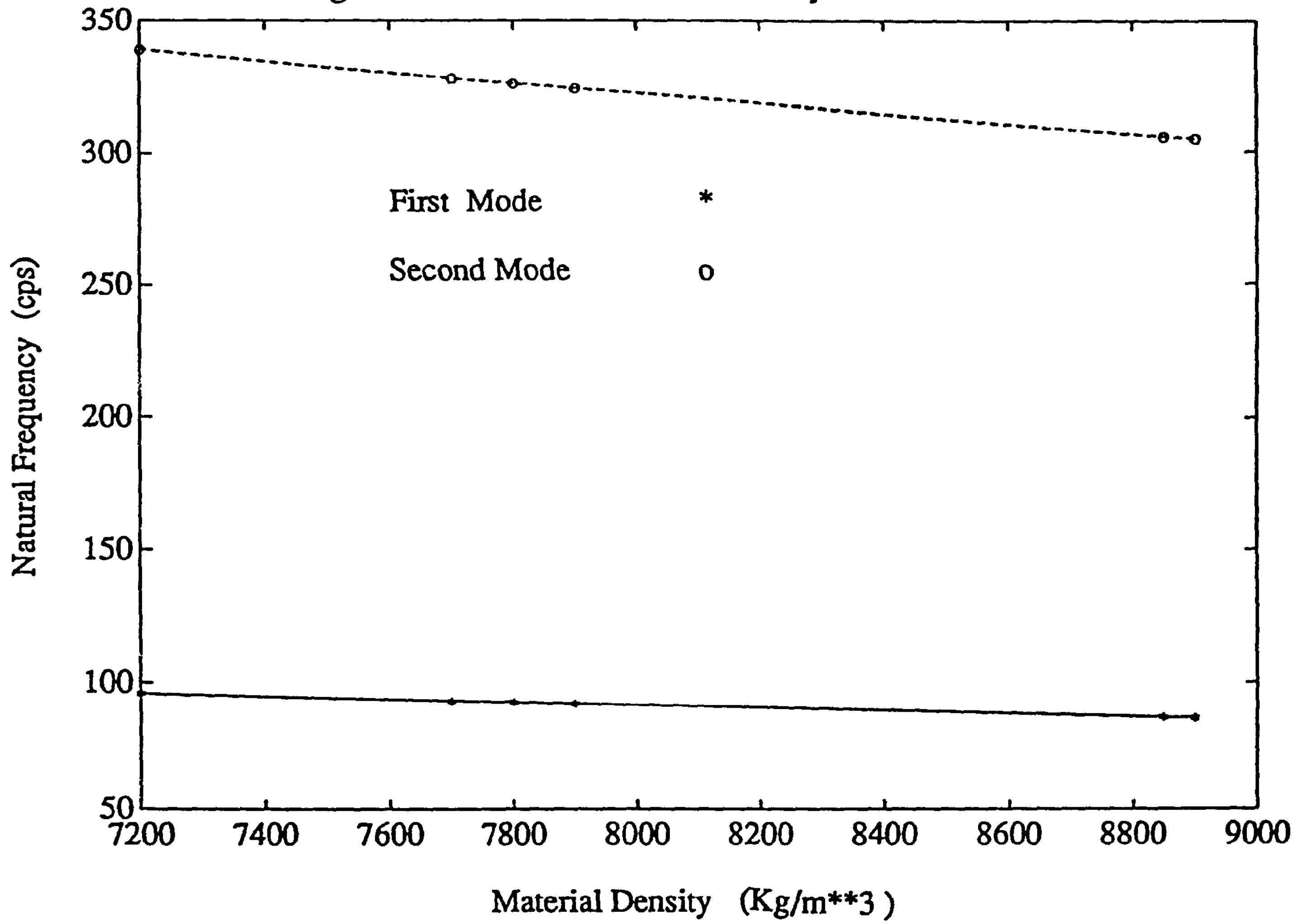

ℓ_2 = 0.266m and ℓ_1 = 0.666m and ℓ_2 = 0.133m) as shown in Fig.4.2.1a, b, c. The natural frequency of the rotor is obtained each time by varying the disk thickness ranging from 0.001 to 0.01 m. For each disk location, the results are recorded in increasing order of frequency of the rotor which can be seen in Tables 4.4.1, 4.4.2, and 4.4.3. The critical speed vs the disk position and disk thickness are then plotted as shown in Fig.4.4.1 and Fig.4.4.2.

It is observed that the natural frequency of the rotor is increased by decreasing the disk thickness regardless of disk location. Fig.4.4.2 shows that the natural frequency of the rotor second mode is constant when the disk is located at the far right end of the rotor. When the disk is located at two different disk locations, the natural frequency corresponding to the second mode increases as the disk location advances from the far right end to the mid section of the rotor. This conclusion is partly correct for the first mode of the rotor as is shown in Fig.4.4.1. Here, as the disk thickness decreases from 0.001 to 0.01m the frequency of the first mode for each individual disk location is increased monotonically. If the disk thickness and the disk location from the far end to the mid-section of the rotor decrease simultaneously, the natural frequency for each disk position will increase relative to each other up to 112 cps which corresponds to 0.03m disk thickness. Beyond this disk thickness the behavior of the system will be

Table 4.4.1

Influence of Different Disk Thickness on Natural Frequency of Undamped Rotor					
No.	Mode 1 (CPS)	Mode 2 (CPS)	Mode 3 (CPS)	Mode 4 (CPS)	t_d (m)
1	91.9202	325.2014	923.3311	926.4951	0.01
2	96.5660	325.2014	923.3311	945.4964	0.008
3	105.0651	325.2014	923.3311	986.0824	0.005
4	112.1441	325.2014	923.3311	1026.8684	0.003
5	118.4899	325.2014	923.3311	1070.1338	0.0015
6	120.8531	325.2014	923.3311	1088.1447	0.001

$E = 2.068E11$ N/m^2

$\rho = 7800$ Kg/m^3

$\ell_1 = 0.666$ m

$\ell_2 = 0.133$ m

Table 4.4.2

Influence of Different Disk Thickness on Natural Frequency of Undamped Rotor					
No.	Mode 1 (CPS)	Mode 2 (CPS)	Mode 3 (CPS)	Mode 4 (CPS)	t_d (m)
1	95.7146	352.0435	589.9467	618.2388	0.01
2	99.6925	357.4934	592.9484	1523.5198	0.008
3	106.6465	368.3134	599.5156	1535.5110	0.005
4	112.1090	378.1177	606.3011	1545.9732	0.003
5	116.7460	387.4461	613.6673	1555.5464	0.0015
6	118.4098	391.0313	616.7769	1559.1245	0.001

$E = 2.068E11$ N/m^2

$\rho = 7800$ Kg/m^3

$\ell_1 = 0.533$ m

$\ell_2 = 0.266$ m

Table 4.4.3

Influence of Different Disk Thickness on Natural Frequency of Undamped Rotor					
No.	Mode 1 (CPS)	Mode 2 (CPS)	Mode 3 (CPS)	Mode 4 (CPS)	t_d (m)
1	105.3120	384.6105	656.8689	997.7249	0.01
2	107.1136	393.6206	673.8302	1004.6517	0.008
3	109.9563	408.4960	709.7357	1022.5291	0.005
4	111.9493	419.1662	743.4778	1045.5464	0.003
5	113.4974	427.4194	774.8350	1076.3480	0.0015
6	114.0238	430.1941	786.2868	1091.1855	0.001

$E = 2.068E11$ N/m^2

$\rho = 7800$ Kg/m^3

$\ell_1 = 0.4$ m

$\ell_2 = 0.4$ m

Fig.4.4.1 Influence of Disk Thickness on N.F of Rotor First Mode

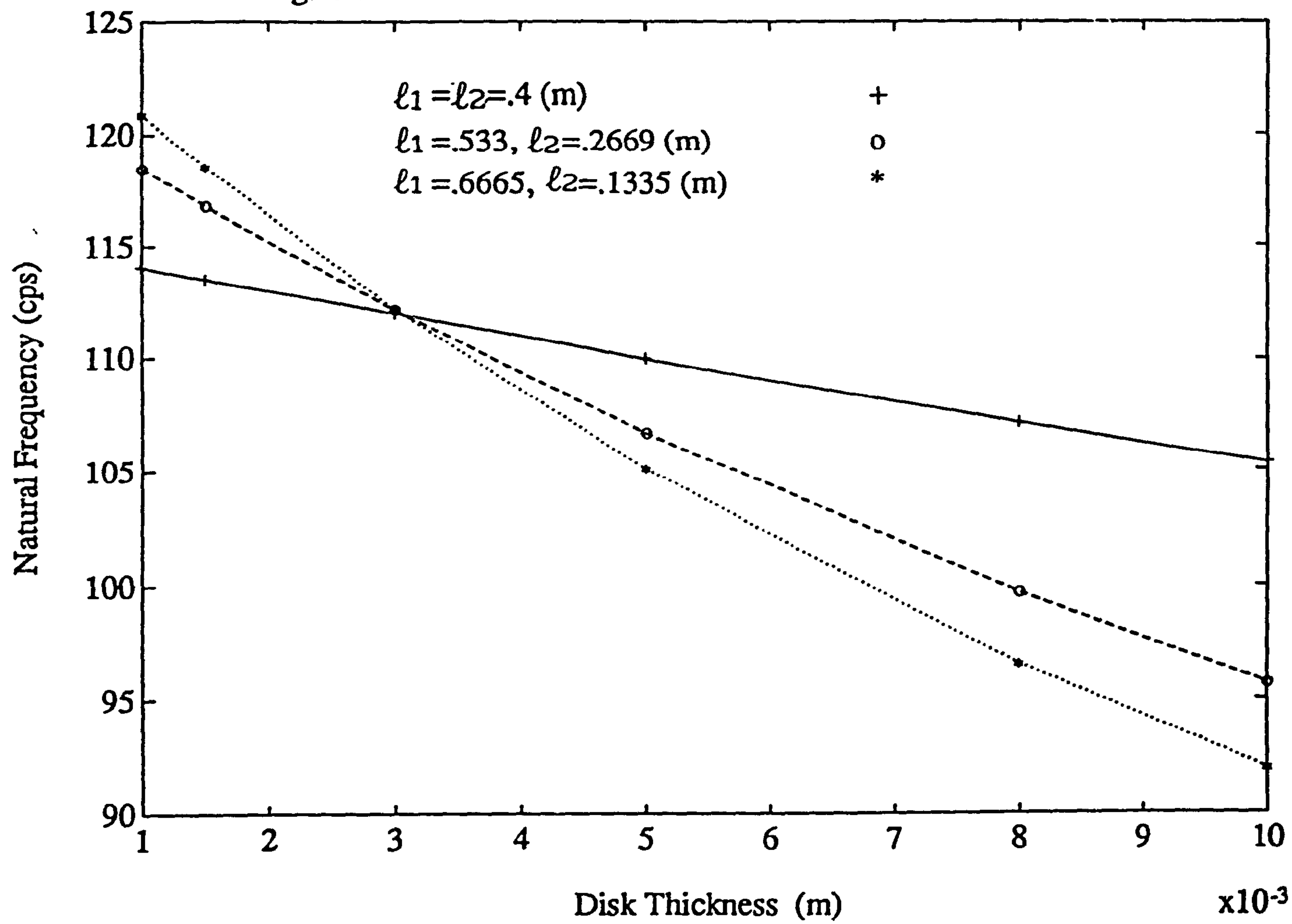

Fig.4.4.2 Influence of Disk Thichness on N.F of Rotor Second Mode

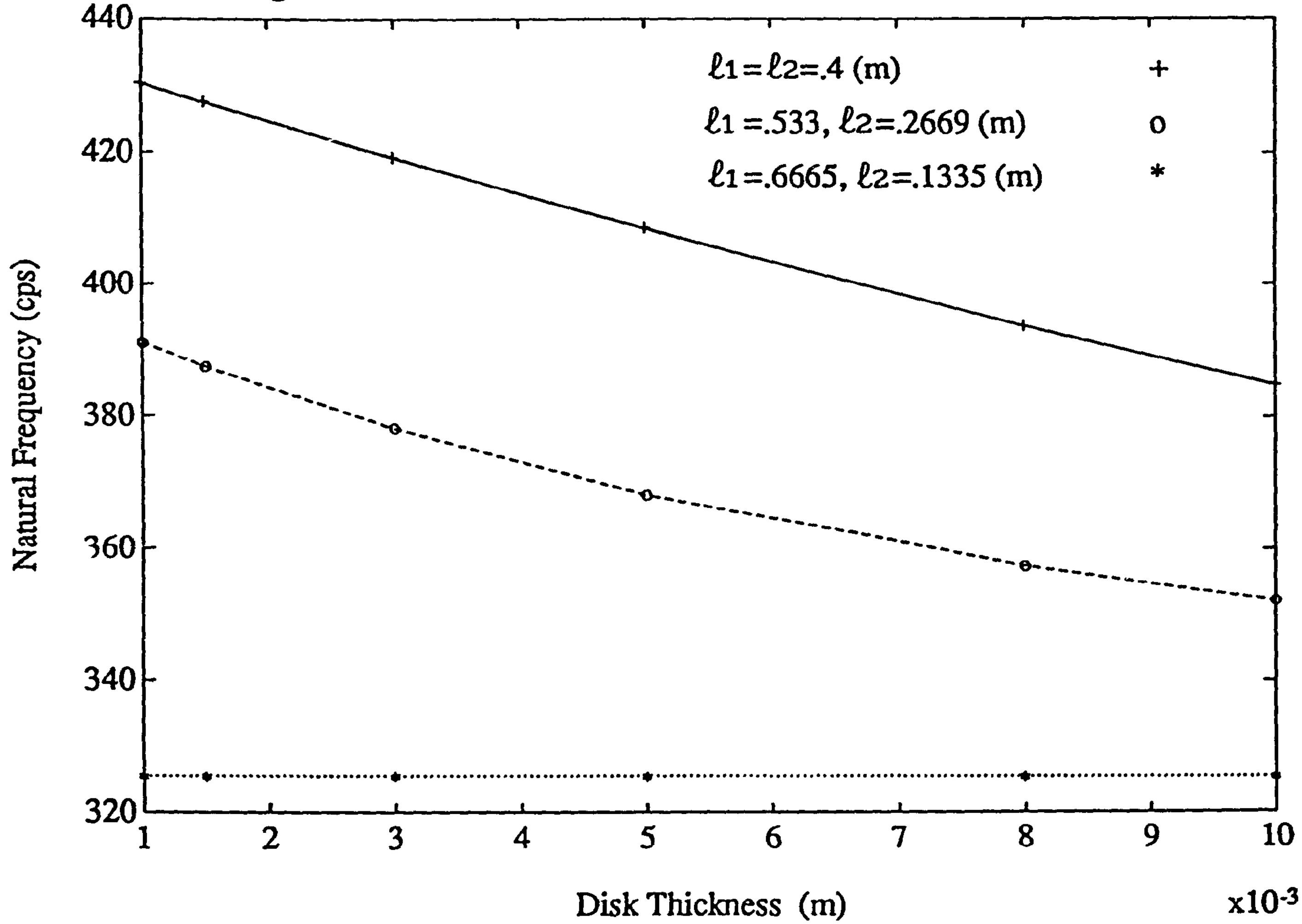

reversed. It is evident that when the disk thickness is 0.003m the rotor will vibrate at 112 cps for all disk locations. Hence, the natural frequency of the system can be altered and controlled by changing the disk thickness and its position.

4.5 Influence of Support Stiffness on Critical Speed of the Rotor

The influence of support stiffness on the critical speed of the rotor is investigated. The rotor is considered to be made up of six equal distance finite elements supported on flexible pedestals as shown in Fig.4.2.1a. The disk is located at the mid-section of the rotor ($\ell_1 = \ell_2 =$ 0.4m)and its thickness remains constant during the simulation. The pedestal and fluid film properties such as the stiffness and damping coefficients are lumped together. The pedestal mass of the rotor support in this analysis is neglected. The result of the computations are obtained for different values of the support stiffness in z direction K_{zz} ranging from $.2K_{yy}$ to $2K_{yy}$ in step of $0.2K_{yy}$ where K_{yy} is equal to 981×10^3 N/m. The value of cross-coupled stiffness K_{zy} is considered to be $0.1K_{yy}$. The support damping is included in the analysis and is equal to $C_{zz} = C_{yy} = 981$ N-sec/m whereas the cross-coupled damping is neglected. The natural frequencies of the first four modes of the rotor are obtained. The results are recorded in increasing order of resonance frequency as presented in Table 4.5.1. A plot of the first four modes of the rotor's critical speed vs the different values of stiffness K_{zz} is shown in Fig.4.5.1.

One can conclude from the result that the natural frequency of the rotor is increased by increasing the value of the ratio K_{zz}/K_{yy}. The increasing natural frequency is only pronounced when the value of the ratio K_{zz}/K_{yy} is increased from 0.2 to 1. When $K_{zz}/K_{yy} = 1$ the natural frequency corresponding to the first, second, third and forth mode of the rotor is recorded to be 53.14, 110.68, 265.76 and 449.32 cps respectively. Beyond the value of $K_{zz}/K_{yy} = 1$ the natural frequency of the system remains almost unchanged. One can, therefore, vary the amount of the support stiffness to control the vibration of the system.

4.6 Influence of Support Damping on Critical Speed of the Rotor

The influence of support damping on the critical speed of the rotor is studied. The rotor is supported by flexible pedestal with a single disk mounted at the mid-point ($\ell_1 = \ell_2 = 0.4$m)of the rotor. The mass of the pedestal for this study is neglected. The thickness of the disk is assumed to be 0.01 m. The configuration of the rotor-bearing system for the present analysis is shown in Fig.4.2.1a. The results of

Table 4.5.1

Influence of Support Stiffness on the damped Critical Speed of the Rotor					
No.	Mode 1 (CPS)	Mode 2 (CPS)	Mode 3 (CPS)	Mode 4 (CPS)	Kzz/Kyy Coeff'nt
1	25.6889	20.5762	226.9754	438.7687	0.2
2	37.4928	61.9154	238.2127	441.5791	0.4
3	44.8508	84.0781	248.8318	444.4107	0.6
4	49.9560	100.1271	258.5016	447.1516	0.8
5	53.1404	110.6839	265.7688	449.3201	1.0
6	54.3098	114.6956	268.7202	450.2284	1.2
7	54.6504	115.8793	269.6112	450.5058	1.4
8	54.7895	116.3649	269.9793	450.6209	1.6
9	54.8629	116.6216	270.1746	450.6820	1.8
10	54.9079	116.7790	270.2945	450.7196	2.0

$E = 2.068E11$ N/m^2

$\rho = 7800$ Kg/m^3

$\ell_1 = 0.4$ m

$\ell_2 = 0.4$ m

$K_{yy} = 981E3$ N/m

$C_{zz} = 981$ N-sec/m

$C_{yy} = 981$ N-sec/m

$C_{zy} = C_{yz} = 0$

$K_{zy} = K_{yz} = 0$

$M_p = 0$

Fig.4.5.1 Influence of Support Stiffness on N.F of Rotor

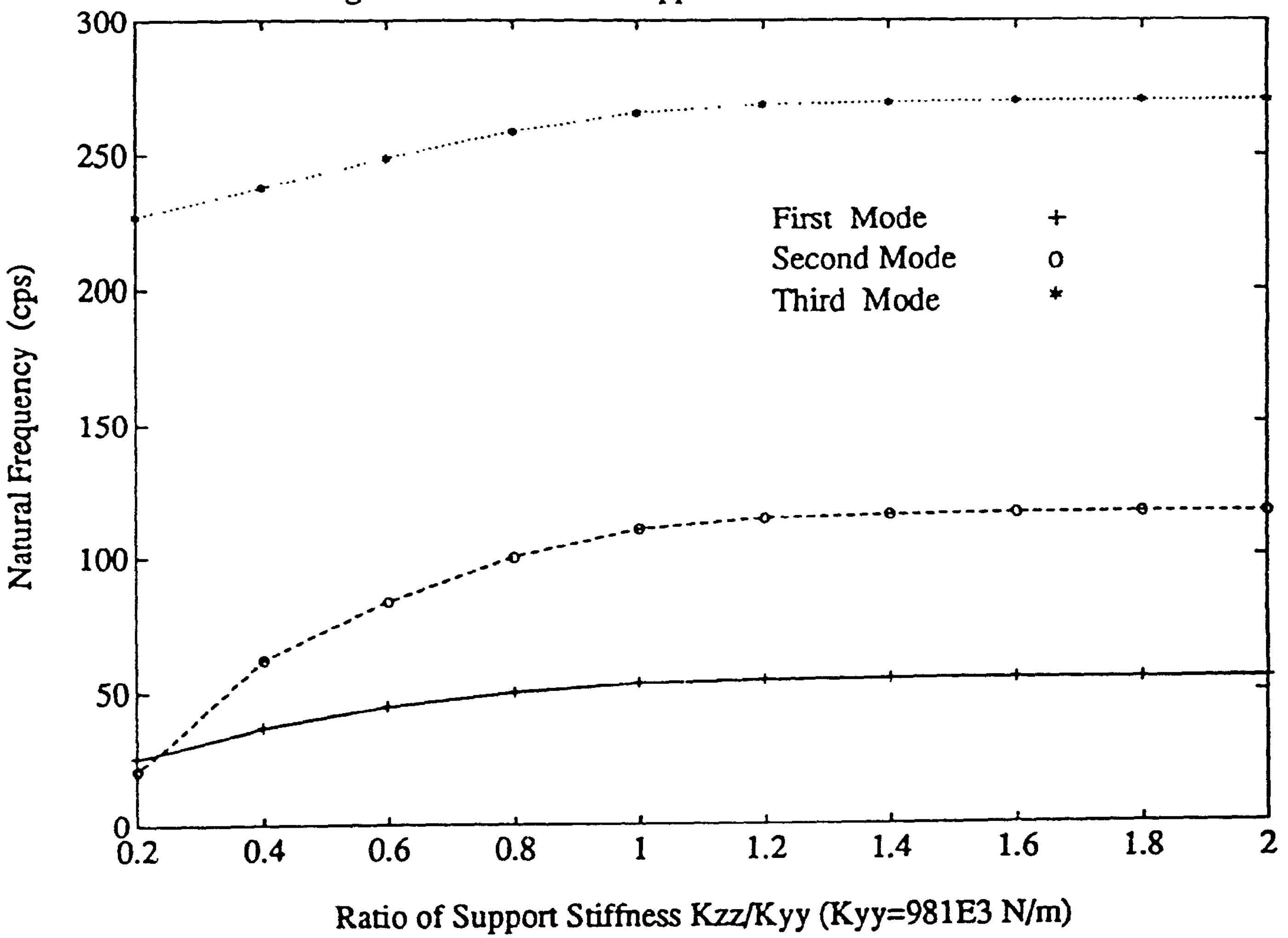

the simulation are obtained for different values of support damping in the direction C_{zz} ranging from $0.2C_{yy}$ to $2C_{yy}$ in steps of $0.2C_{yy}$. The value of C_{yy} remains constant and equal to 981 N-sec/m. The support stiffness cross coupling is included in the analysis and is considered to be 981×10^2 N/m. The cross-coupling of the support damping is neglected. The results of the first four modes for different levels of support damping are presented in increasing order of resonance frequency in Table 4.6.1. A plot of the recorded damped critical speed vs the different levels of support damping is shown in Fig.4.6.1.

Increasing the ratio C_{zz}/C_{yy} from 0.2 to 2 does not show a significant influence on the response of the system. The maximum frequency fluctuation for the first and second mode are of the order of 2 and 9 cps respectively. As the ratio C_{zz}/C_{yy} increases the natural frequency of the first and second mode of the system first decreases and then increases back again; whereas, the frequency of the third and higher modes decrease monotonically at a lower rate. Support damping is, therefore, considered to be another factor in controlling the response of the system. It is important to mention that any change to the damping coefficient has a significant effect on the stability of the system. This effect is not addressed in the present analysis.

Table 4.6.1

Influence of Support Damping on the Critical Speed of the Rotor					
No.	Mode 1 (CPS)	Mode 2 (CPS)	Mode 3 (CPS)	Mode 4 (CPS)	Czz/Cyy (Ratio)
1	54.8048	122.6856	270.6952	450.8894	0.2
2	54.4792	122.2988	270.6634	450.8945	0.4
3	53.5387	116.2097	270.5962	450.9046	0.6
4	53.1874	113.6443	270.3282	450.9350	0.8
5	53.1404	110.6839	265.7688	449.3201	1.0
6	53.3517	110.5530	264.0053	446.8212	1.2
7	53.8932	108.7584	256.4281	441.7036	1.4
8	54.9348	118.1553	246.6319	435.5542	1.6
9	55.4272	117.9498	234.2725	428.2687	1.8
10	55.3274	117.8362	218.5852	419.7953	2.0

$E = 2.068E11$ N/m^2

$\rho = 7800$ Kg/m^3

$\ell_1 = \ell_2 = 0.4$ m

$K_{yy} = K_{zz} = 981E3$ N/m

$K_{yz} = K_{zy} = 981E2$ N/m

$C_{zz} = C_{yy} = 981$ N-sec/m

$C_{zy} = C_{yz} = 0$

$M_p = 0$

Fig.4.6.1 Influence of Support Damping on N.F of Rotor

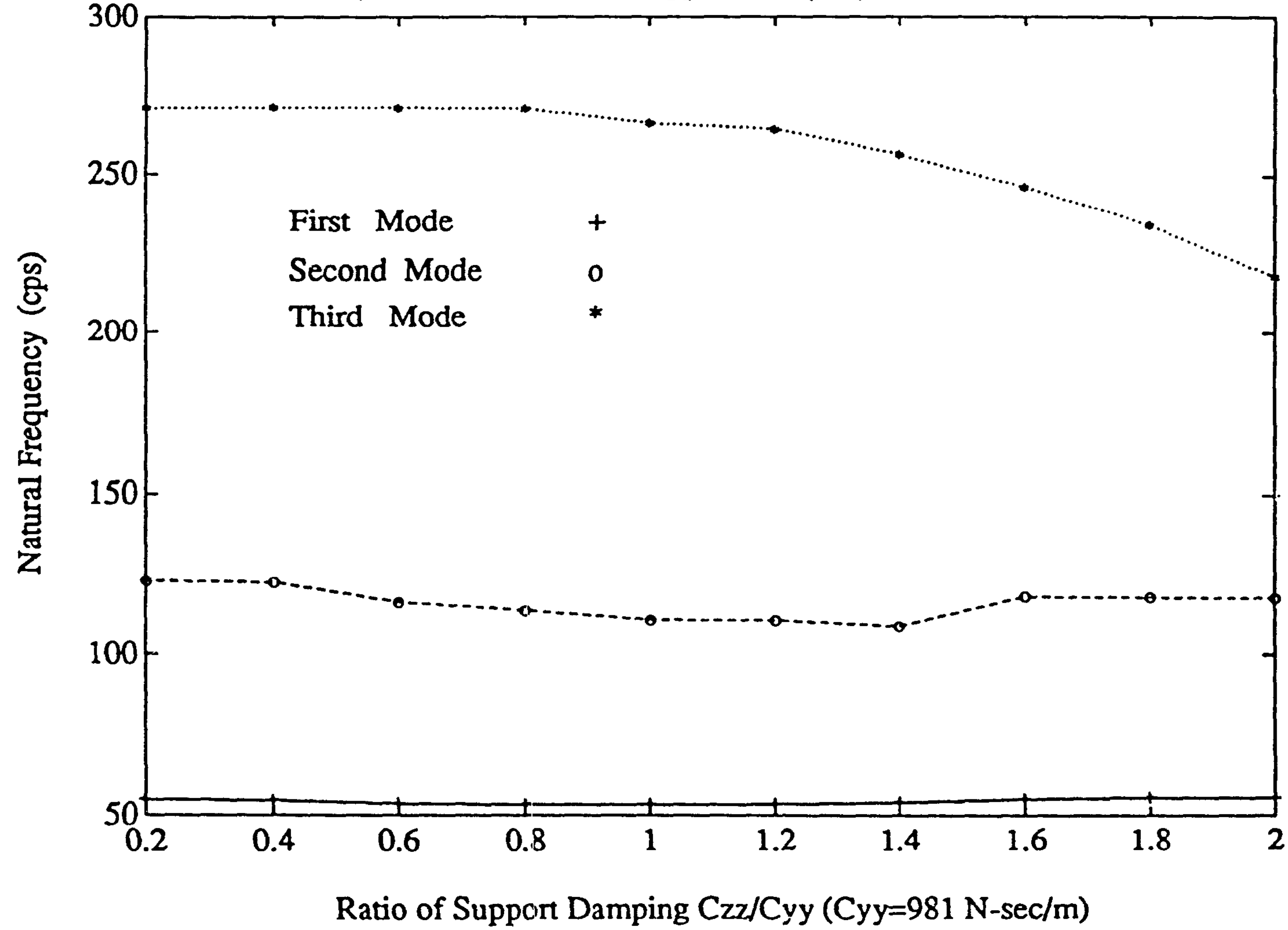

4.7 Influence of Pedestal Mass on Critical speed of the Rotor

The influence of pedestal mass on the critical speed of the rotor is investigated by considering the flexible rotor mounted on a flexible pedestal. The disk is located at the mid-span of the rotor ($\ell_1 = \ell_2 = 0.4$m). The disk thickness and disk location are held constant throughout the calculation. The disk thickness is assumed to be 0.01m. The rotor bearing pedestal configuration for this analysis is shown in Fig.4.7.1. Only the pedestal stiffness in Z direction is considered in this analysis and it is assumed to be $Kzz_p = 3.55 \times 10^8$ N/m (20.272×10^5 lb/in) [37]. The pedestal damping is considered to be negligible. The fluid film properties are taken as $Kzz = Kyy = 981 \times 10^3$ N/m and $Czz = Cyy = 981$ N-sec/m and the cross coupling is neglected. The computations are obtained for the various values of pedestal mass ranging from 0.68 to 462 kg. The properties of the rotor material are listed in Table 4.7.1. The results of the calculations are presented in increasing order of resonance frequency in Tables.4.7.2, 4.7.3, and 4.7.4. Finally, a plot of the critical speed vs the different values of pedestal mass are shown in Fig .4.7.2, 4.7.3, 4.7.4.

The result of the simulation for the three different rotor material densities has clearly shown that the pedestal mass does not have any significant effect on the first mode

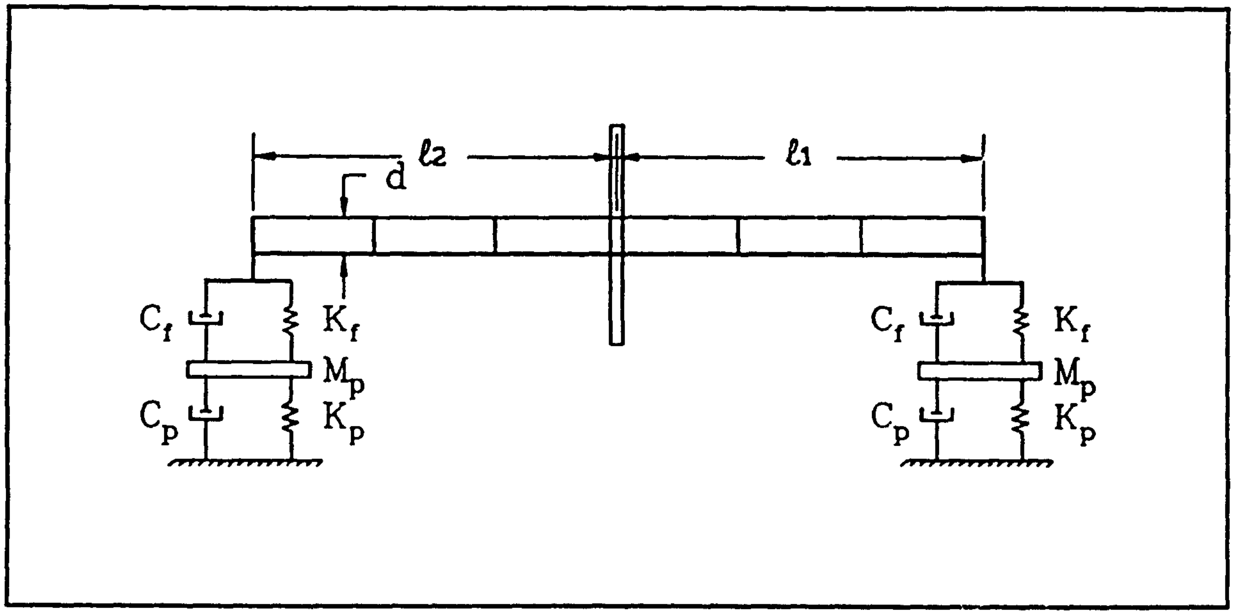

Fig.4.7.1 Simply supported rotor–bearing–pedestal system with a single disk mounted on its mid–section

Table 4.7.1

Material Properties of the Rotor		
Material	Density kg/m^3	Modulus of E N/m^2
Aluminum	2700	6.895×10^{10}
Steel (430)	7800	2.068×10^{11}
Brass	8500	1.103×10^{11}

Table 4.7.2

Influence of Pedestal Mass on the Critical Speed of the Rotor					
No.	Mode 1 (CPS)	Mode 2 (CPS)	Mode 3 (CPS)	Mode 4 (CPS)	M_P/M_R
1	73.38	220.5	268.60	371.38	0.177
2	73.38	220.5	268.60	371.38	0.474
3	73.37	219.96	268.60	371.38	1.066
4	73.37	219.96	362.97	268.60	1.777
5	73.37	219.96	314.52	268.60	2.370
6	73.37	222.3	219.96	268.60	4.740
7	73.37	157.24	219.96	268.60	9.481
8	73.37	99.5	219.96	268.60	23.70
9	44.50	73.42	219.96	268.60	118.51

$E = 6.89E10$ N/m^2

$\rho = 2700$ Kg/m^3

$\ell_1 = \ell_2 = 0.4$ m

$t_d = 0.01$ m

$K_{yy} = K_{zz} = 981E3$ N/m

$K_{yz} = K_{zy} = 0$ N/m

$C_{zz} = C_{yy} = 981$ N-sec/m

$C_{p_z} = 0$

$K_{p_z} = 3.55E8$ N/m

Table 4.7.3

Influence of Pedestal Mass on the Critical Speed of the Rotor					
No.	Mode 1 (CPS)	Mode 2 (CPS)	Mode (CPS)	Mode 4 (CPS)	M_P/M_R
1	55.0423	117.4055	270.78	450.8743	0.061
2	55.0421	117.4080	270.78	450.8743	0.164
3	55.0418	117.4133	270.78	450.8743	0.369
4	55.0414	117.4206	270.78	362.9920	0.615
5	55.0410	117.4276	270.78	314.2647	0.820
6	55.0396	117.4646	222.67	270.7871	1.64
7	55.0365	117.4232	157.34	270.7871	3.28
8	55.025	99.4247	117.42	270.7651	8.204
9	44.453	55.0915	117.42	270.7825	41.024

$E = 2.608E11$	N/m^2
$\rho = 7800$	Kg/m^3
$\ell_1 = \ell_2 = 0.4$	m
$t_d = 0.01$	m
$K_{yy} = K_{zz} = 981E3$	N/m
$K_{yz} = K_{zy} = 0$	N/m
$C_{zz} = C_{yy} = 981$	N-sec/m
$C_{p_z} = 0$	
$K_{p_z} = 3.55E8$	N/m

Table 4.7.4

Influence of Pedestal Mass on the Critical Speed of the Rotor					
No.	Mode 1 (CPS)	Mode 2 (CPS)	Mode (CPS)	Mode 4 (CPS)	M_P/M_R
1	46.51	112.46	212.9	321.44	0.056
2	46.51	112.46	212.9	321.44	0.1505
3	46.51	112.47	212.9	321.44	0.338
4	46.51	112.52	212.9	321.44	0.5646
5	46.51	112.47	212.9	314.9	0.7529
6	46.51	112.49	222.3	212.9	1.505
7	46.51	112.58	157.42	212.9	3.011
8	46.50	99.40	112.52	212.9	7.529
9	44.39	46.54	112.52	212.9	37.64

$E = 2.608E11$ N/m^2

$\rho = 10150$ Kg/m^3

$\ell_1 = \ell_2 = 0.4$ m

$t_d = 0.01$ m

$K_{yy} = K_{zz} = 981E3$ N/m

$K_{yz} = K_{zy} = 0$ N/m

$C_{zz} = C_{yy} = 981$ N-sec/m

$Cp_z = 0$

$Kp_z = 3.55E8$ N/m

Fig.4.7.2 Influence of Pedestal Support on N.F of Aluminum Rotor

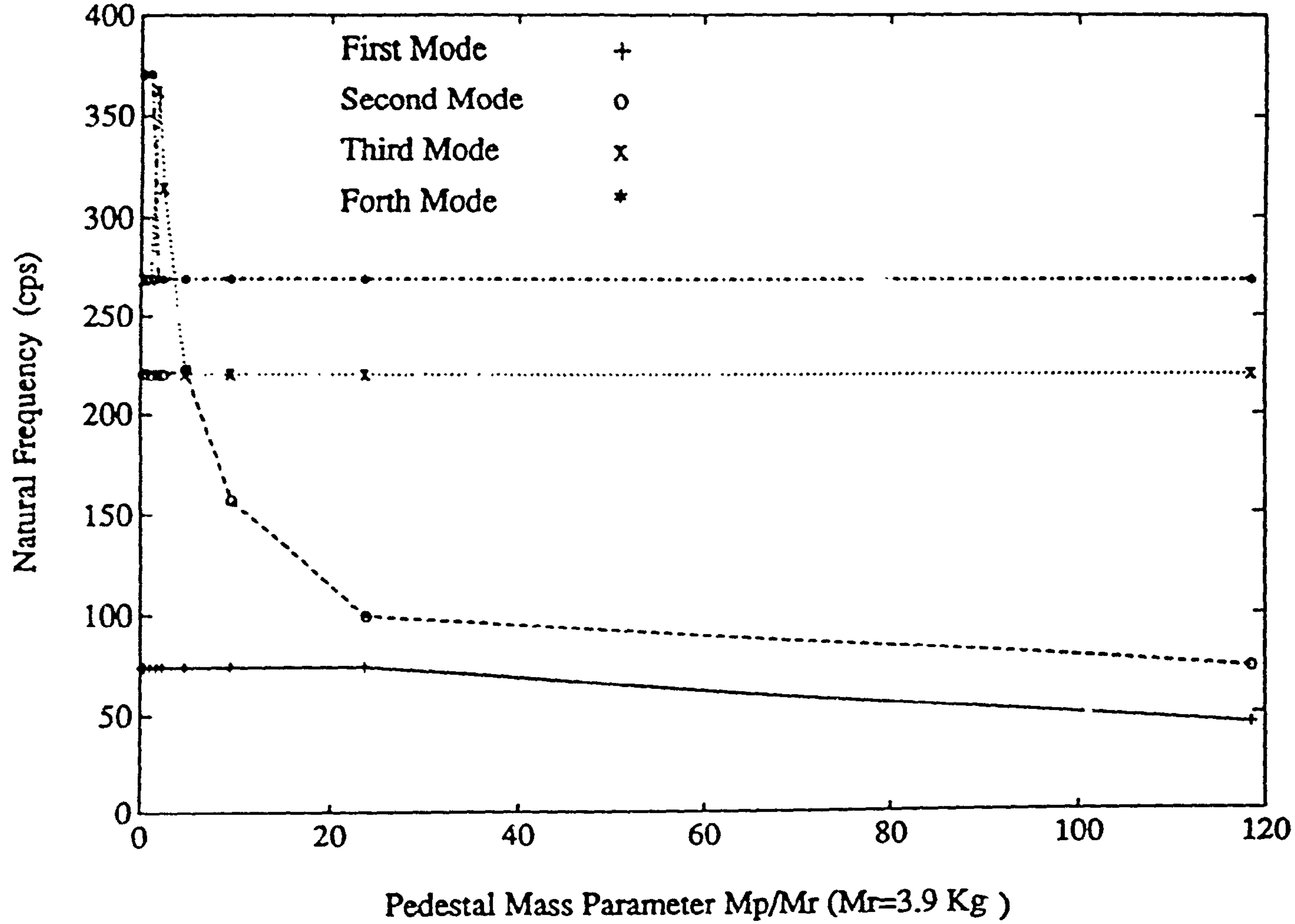

Fig.4.7.3 Influence of Pedestal Support on N.F of Steel Rotor

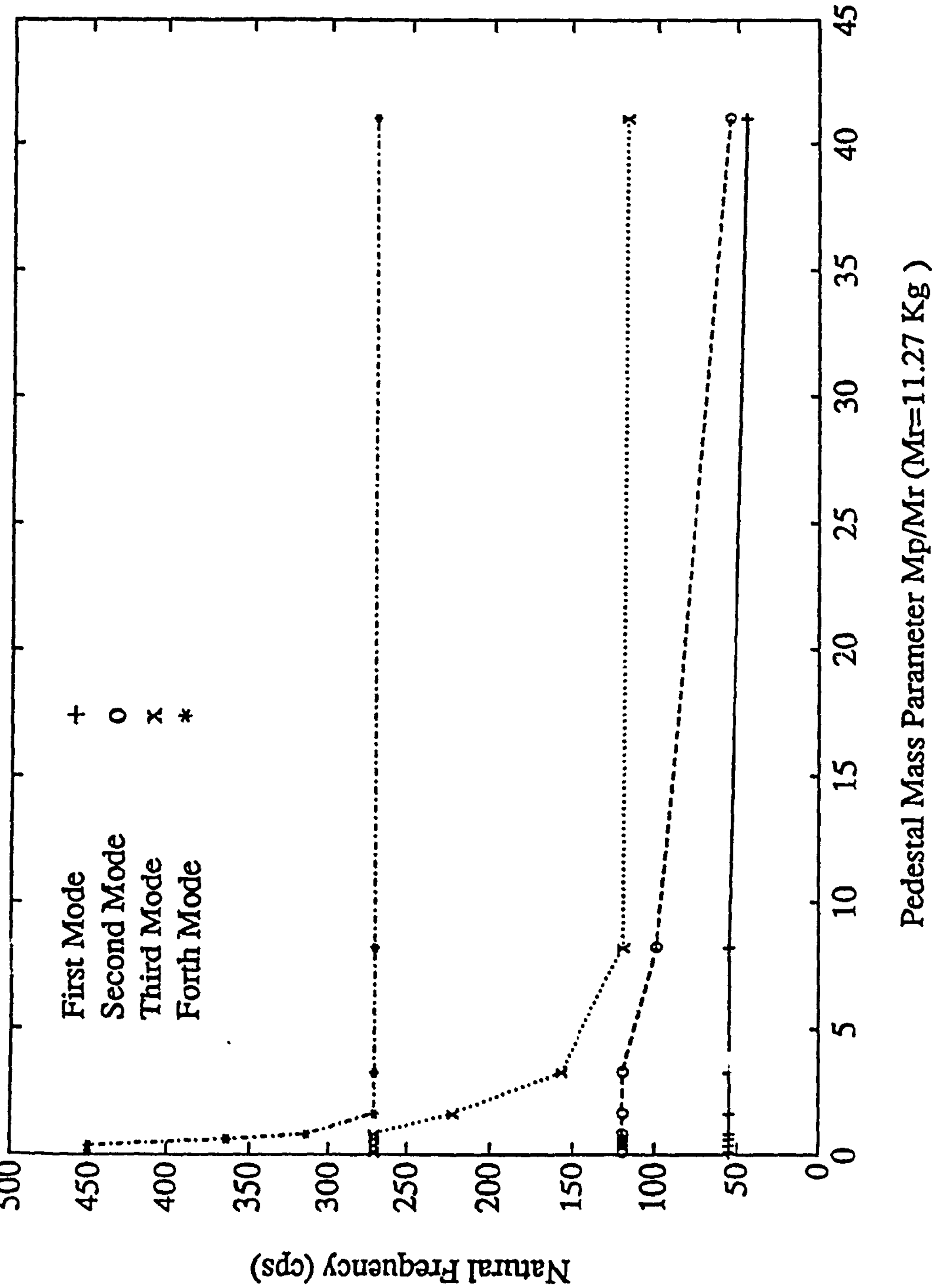

Fig.4.7.4 Influence of Pedestal Support on N.F of Brass Rotor

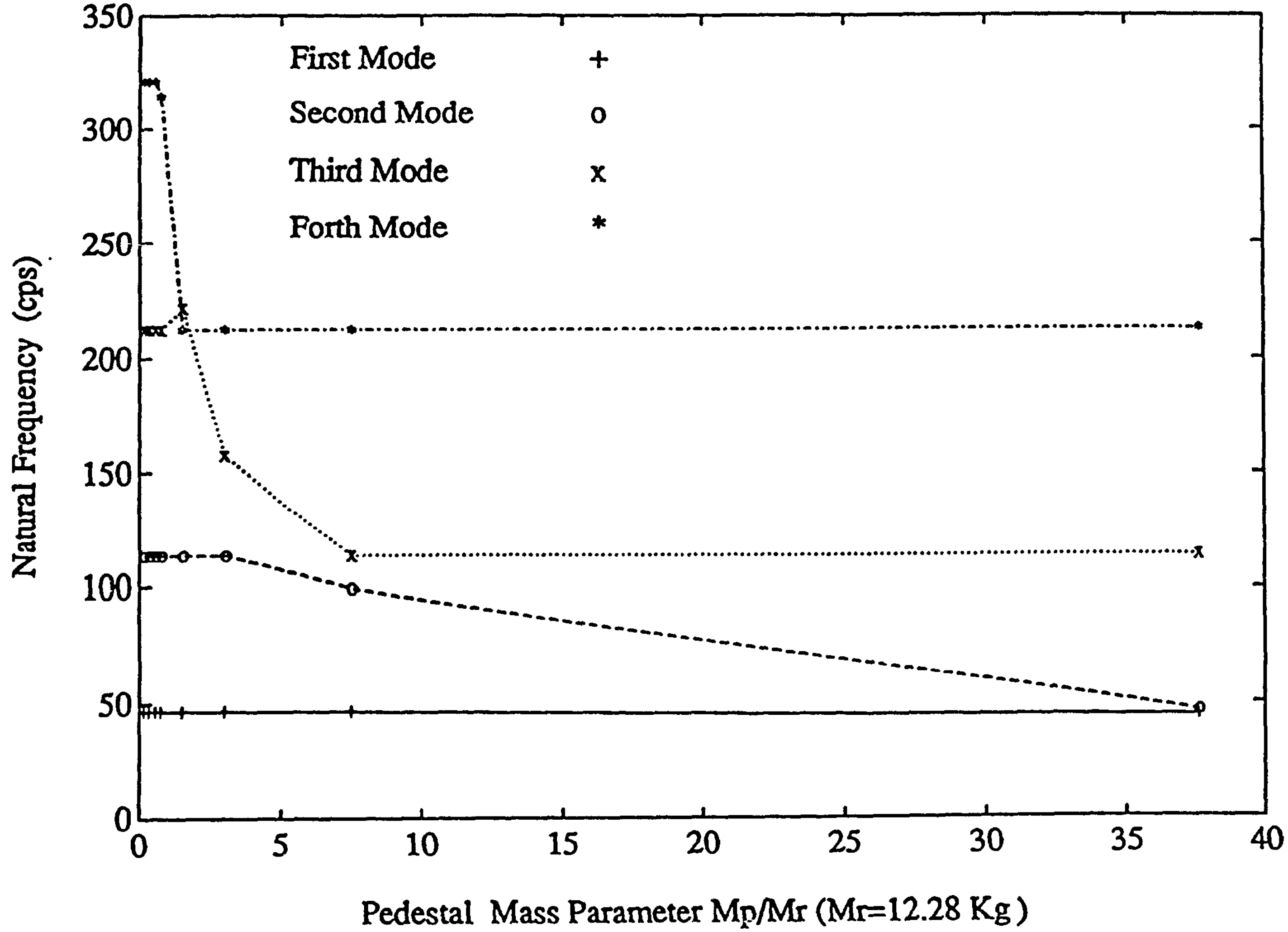

of the system. The increasing pedestal mass has also shown little effect on the second mode of the system. Although these changes are very small, a rotor with lower material density is more susceptible to bring down the natural frequency of the system. The pedestal mass has a significant effect on the third, fourth and higher modes of the system. Consider that as the pedestal mass parameter for aluminum rotor increases from 0.06 to 10. as shown in Fig 4.7.2, the resonance frequency of the rotor third mode decreases from 268.6 to 219.9 cps with the difference of 48.7 cps. These differences are higher when material density increases. For example, the third mode natural frequency of the system of steel rotor is decreased from 270.78 to 117.4 cps with the difference of 153.4 cps and brass rotor with the difference of 100.4 cps. It is also observed that for aluminum rotor the natural frequency of the first mode with pedestal mass parameter of 0.177 is equal to the natural frequency of the second mode when the pedestal mass parameter is equal to 118.5. Similarly, the natural frequency of the second mode with pedestal mass parameter of 0.177 is equal to the natural frequency of the third mode with pedestal mass parameter of 181.5 and so on. These effects are also illustrated for rotors with different materials as shown in Fig.4.7.3, 4.7.4. It is, therefore, important to consider the pedestal mass to improve the performance of the rotor-bearing-pedestal system.

4.8. Discussion of results

The parametric study of a single disk rotor-bearing-pedestal system supported on hydrodynamic bearings is studied using the component mode synthesis technique. Even though a single disk rotor-bearing-pedestal with a few finite elements is chosen, a large system with several disks, impellers, mechanical coupling and bearings can be treated equally. By this technique the size of the overall finite element system matrices can be substantially reduced without affecting the dynamic characteristics of the system response.

The rotor mass and stiffness are represented by means of Archer's [8] consistent formulation. The model includes the effects of rotary inertia only. The effect of gyroscopic moment, shear deformation and axial torque are not included in the analysis. However these effects can be included as per the references [9,32]. In this analysis the rotational fluid film coefficient is neglected. Also, only pedestal mass and stiffness in Mp_z and Kp_z are considered in this analysis.

The response of the rotor-bearing-pedestal system depends on many factors some of which are examined in detail in the previous chapter. The configuration of a single rotor supported on hydrodynamic bearings at both ends can be altered by adjusting the bearing properties and the location of the disk so as to have a specific load distribution on the two bearings, varying the density of the rotor, increasing the mass of pedestal etc. Consequently, the response pattern of the rotor changes depending upon the rotor configuration.

Significant response in the vertical direction can occur when the rotor experiences changes in such support properties as stiffness and damping. The parametric study of rotor-bearing-pedestal system is an efficient tool for an engineer designer to optimize the performance of rotor-bearing-pedestal system so as to avoid critical speed condition in the vicinity of operating speed.

CHAPTER 5

CONCLUSION

5.1 Concluding Remarks

The thesis has examined the general problem of rotor dynamics. After reviewing the current methods available it is found that there is a need for a computationally efficient and accurate method which can handle all the usual complexities like flexibility of bearings, pedestals etc. It is recommended that the component mode synthesis method is appropriate for this purpose and is developed to study the rotor-bearing-pedestal behavior. With component mode synthesis method proposed in this thesis the size of system matrices can be reduced considerably without affecting the dynamic characteristics of the system response. A general purpose digital computer program **SETSA** is developed and is fully described. The accuracy of the method as well as the program capability with reference to actual examples are established. An extensive study of the influence of support flexibility on the critical speed of the rotor is made, and useful practical conclusions are obtained. The computer program has also the capability to perform similar calculations to study the influence of any prescribed ground motion on the dynamic system.

The digital computer program **SETSA** is developed in chapter 3 to obtain the parametric study of rotor-bearing-pedestal system based on component mode synthesis. The user may bypass the CMS option and proceed directly with the finite element method provided that the size of the program does not exceed the computer limitations. The structure may consist of a maximum of 4 components, each of which may contain up to a total of 10 elements characterized by different element length and diameter. This will allow the user reasonable flexibility in modeling a system with several geometric discontinuities. Non symmetric support properties such as damping can be easily accommodated by the program.

The accuracy of the program is tested with two actual examples and the results of the simulation are obtained for different levels of mode truncation. The percentage of error resulting from mode truncation is then tabulated. The computer program **SETSA** is finally used to study the influence of such effects as: stiffness parameter, material density of the rotor with constant modulus of elasticity, different disk thickness and disk location, support stiffness and damping, and pedestal mass on critical speed of the rotor. Hence, the program developed may also serve as an essential component of an active control system in which the support dampings and stiffnesses may be conveniently defined.

The analysis is made on the basis of a linear elastic rotor spinning at a constant speed and external viscous damping is provided only at the supports. No high temperature effects are included. Although the program **SETSA** is designed to handle linearly elastic supports, with only a minor modification, an analysis with nonlinear support properties is possible. It is observed in parametric study of different disk thickness and disk location variation that all the curves passes through one point when the disk thickness is 3.1 mm regardless of disk location. Also a jump is observed in the natural frequency of third and higher modes in parametric study of pedestal mass variation. The reason for these phenomena is not clear and need further investigation. Mode truncation criteria should be investigated specifically relating to the damped modes in the complex normal mode development. There is still not mathematically proven which mode should be truncated to get better results and yet guarantee convergence. This is also requires further investigation.

REFERENCES

1. Jeffcotte, H. H., "The Lateral Vibration of Loaded Shafts in Neighborhood of a Whirling Speed - The Effect of Want of Balance", Philosophical Magazine, 37 (6), 1919, p. 304.

2. Prohl, M. A., "A General Method for Calculating Critical Speeds of Flexible Rotors", Transactions of ASME, Journal of Applied Mechanics, 12, 1945, pp. 142-148.

3. Lemke, D. G. and Trumpler, P. R., "On the Dynamic Response of Axially Coupled Turborotors", Journal of Engineering for Industry, May 1972 p.507-516.

4. Bishop, R. E. and Parkinson, A. G., "Vibration and Balancing of Flexible Shafts", Applied Mechanic Reviews, 21 (5), May, 1968, p.439.

5. Lund, J. W., "Modal Response of Flexible Rotor in Fluid Film Bearing", Trans: of ASME Journal of Eng for Industry, 96, 1974, p.525.

6. Bhat, R. B., Subbiah, R. and Sankar, T. S., "Dynamic Behavior of Simple Rotor with Dissimilar Hydrodynamic Bearings by Modal Analysis", Trans: of ASME: Journal of

Vibration, Acoustics, Stress and Reliability, in Design, 107 (2), April, 1985, pp.267-269.

7. Ruhl, R. L., and Booker, J. F., "Finite Element Model for Distributed Parameter Turborotor System", ASME Tran Feb. 1972, p. 126

8. Archer, John S., "Consistent Mass Matrix for Distributed Mass Systems", Journal of Structural Division Proceeding of the American Society of Civil Engineers, Aug, 1963, p.161.

9. Nelson, H. D., and McVaugh, J. M., "The Dynamics of Rotor Bearing Systems Using Finite Elements", Journal. of Eng. for Industry, 98 (2), 1976, p.593.

10. Zorzi, E. S., and Nelson, H. D., "Finite Element Simulation of Rotor-Bearing System with Internal Damping", Journal of Engineering for Power, Jan, 1977, p.71.

11. Nelson H. D., "A Finite Rotating Shaft Element using Timoshenko Beam Theory", Trans: of ASME: Journal of Mechanical Design, 102, 1980, pp.793-803.

12. Zorzi, E. S., and Nelson, H. D., "The Dynamics of Rotor Bearing System with Axial Torque (A Finite Element Approach)", Journal of Mechanical Design, Trans: of

ASME: 102, Jan, 1980, pp.158-161.

13. Guyan, R. J., "On the Reduction of Stiffness and Mass Matrices", American Institute of Aeronautics and Astronautics Journal, 380 (3), 1965.

14. Hurty, W. C., "Vibration of Structural System by Component Mode Synthesis",ASCE: journal of Engineering Mechanical Divisions, 86, August, 1960, pp.51-69.

15. Hurty, W. C., "Dynamic Analysis of Structural Systems Using CMS", AIAA journal, 3 (4), 1965, p.678.

16. Glandwell, G. M. L., "Branch Mode Analysis of Vibration Systems", Journal of Sound and Vibration, 1, 1964, pp.41-59.

17. Craig, R. R. and Chang, C. J., "A Review of Substructure Coupling Methods for Dynamic Analysis", Advance in Engineering Science, NASA: cp-2001, 2, Nov, 1976, pp.393-408.

18. Craig, R. R. Mervyn C. C. and Bampton., "Coupling of Substructures for Dynamic Analysis", AIAA journal, 6 (7), July, 1968, p.1313.

19. Rubin, S., "Improved C.M. Representation for Structural Dynamic analysis," AIAA Journal, 13 (8), Aug, 1975,

p.995.

20. Kuhar,E. J. Stahle, Stahle, C. V., "Dynamic Transformation Method for Modal Synthesis", AIAA Journal, 12 (5),1974

21. Hintz,R. M., "Analytical Methods in Component Modal Synthesis", AIAA Journal, 13 (8), Aug, 1975 pp 1007-1016

22. Hasselman, T. K. and Kaplan., "Dynamic Analysis of Large System by Complex Mode Synthesis", ASME: Journal of Dynamic System, Measurement and Control, 96 (3) Sept 1974, pp.327-333.

23. Glasgow, D.A., "Analysis of Rotor Bearing System Using Component Mode Synthesis", PhD Dissertation ,Arizona State University, 1981

24. Craig Jr, R. R., Chung Yung-Tseg., "Generalized Substructure Coupling Procedure for Damped System," AIAA Journal, 20 (3), 1982, pp.442-444.

25. Masaaki ookuma akio., Bull, JSME 29 (253),1986.

26. Benfield, W. A. ,Hruda, R. F., "Vibration Analysis of Structures by Component Mode Substitution", AIAA Journal, 9 (7), July, 1977, p.1255.

27. Meirovitch, L. and Hale A. L., "On the Substructure Synthesis Method", AIAA journal 9, July, 1981, pp.940-947.

28. Meirovitch, L. and Hale, A. L., "A procedure for Improving Discrete Substructure Representation in Dynamic Synthesis", AIAA journal, 20, Aug, 1982.

29. Meirovitch, L., "A New Method of Solution of the Eigenvalue Problem for Gyroscopic Systems", AIAA journal, 12 (10), 1974, pp.1337-1342.

30. Zheng, Z. C. et, al., "Gyroscopic Mode Synthesis in the Dynamic Analysis of a Multi-Shaft Rotor-Bearing System", Department of Engineering Mechanics, Tsinghua University, beijing, Shenyang Aero Engine Research Institute, Shenyang, 1985.

31. Glasgow, D. A. Nelson H. D., "Stability Analysis of Rotor-Bearing Systems using CMS", Trans: of ASME: 102, April 1980,p.352.

32. Nelson, H. D., Meacham, W. L., and Russell, S. J., "Transient Response of Rotor-Bearing System Using CMS", Department of Aerospace Engineering and Engineering Science Arizona State University ,March, 1981.

33. Craggs, A., "A Component Mode Method for Modeling the

Dynamic of Turbo-Generator Sets", Journal of Sound and Vibration, 117 (2), 1987, pp.277-288.

34. Morton, P. G., "Analysis of Rotors Supported on Many Bearings", Journal of Mechanical Engineering Science, 14, pp.25-33.

35. Gong, H., Chang, H. Y., Huang, H. Y., and Zheng, C. H., "Dynamic Analysis and Experiments of Rotor-Bearing Foundation System for Large Steam Turbine-Generator Set," Shanghai Power Plant Equipment Research Institute Tsinshva University Beijing.

36. Kramer, E. Technische Hochschule Darmstadt, German Federal Republic., "Computation of Vibration of the Coupled System Machine - Foundation", Vibration in Rotating Machinery, Paper C 300/80 1980

37. Subbiah, Rajagopal., "Dynamic Behavior of Rotor Systems with a Comprehensive Model for the Hydrodynamic Bearing Supports using Modal Analysis and Testing", PH.D. Thesis, Department of Mechanical Engineering Concordia University, Aug, 1985.

38 IMSL MATH/LIBRARY,1, Chapter 1-2, Houston, Texas USA

39. Lund, J. W., "Stability and damped critical speeds of a flexible in fluid film bearings", Journal of

Engineering for Industry, May, 1974, pp.509-517.

40. Noriaki, Hagiwara, and Mitsuho, Yoneyama., "Vibration of an asymmetrically Mounted rotor with coupled of a flexible disk", Mechanical Engineering Research Laboratory, Hitachi Ltd, Tsuchiura.

APPENDIX A

FLOW CHARTS

A. 1 Program MAIN

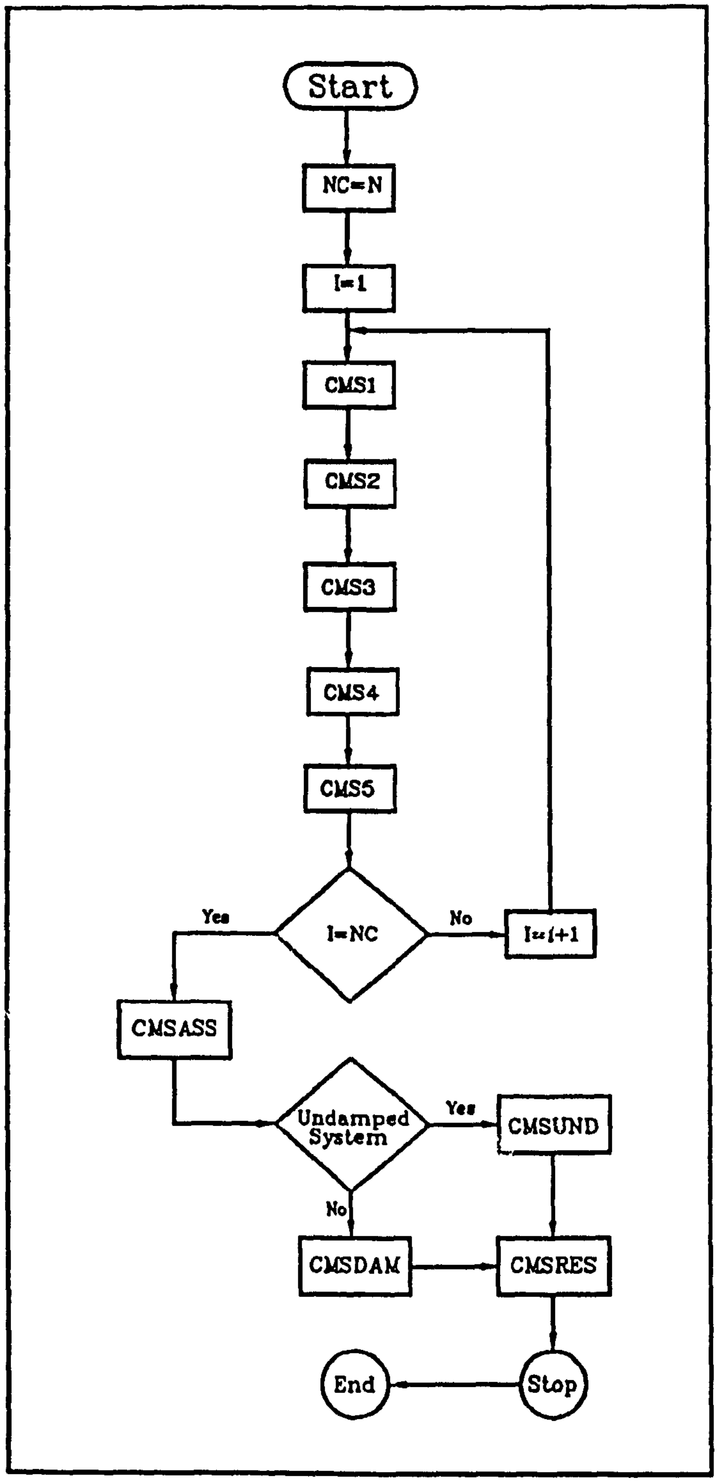

A. 2 Sub-Program CMS1

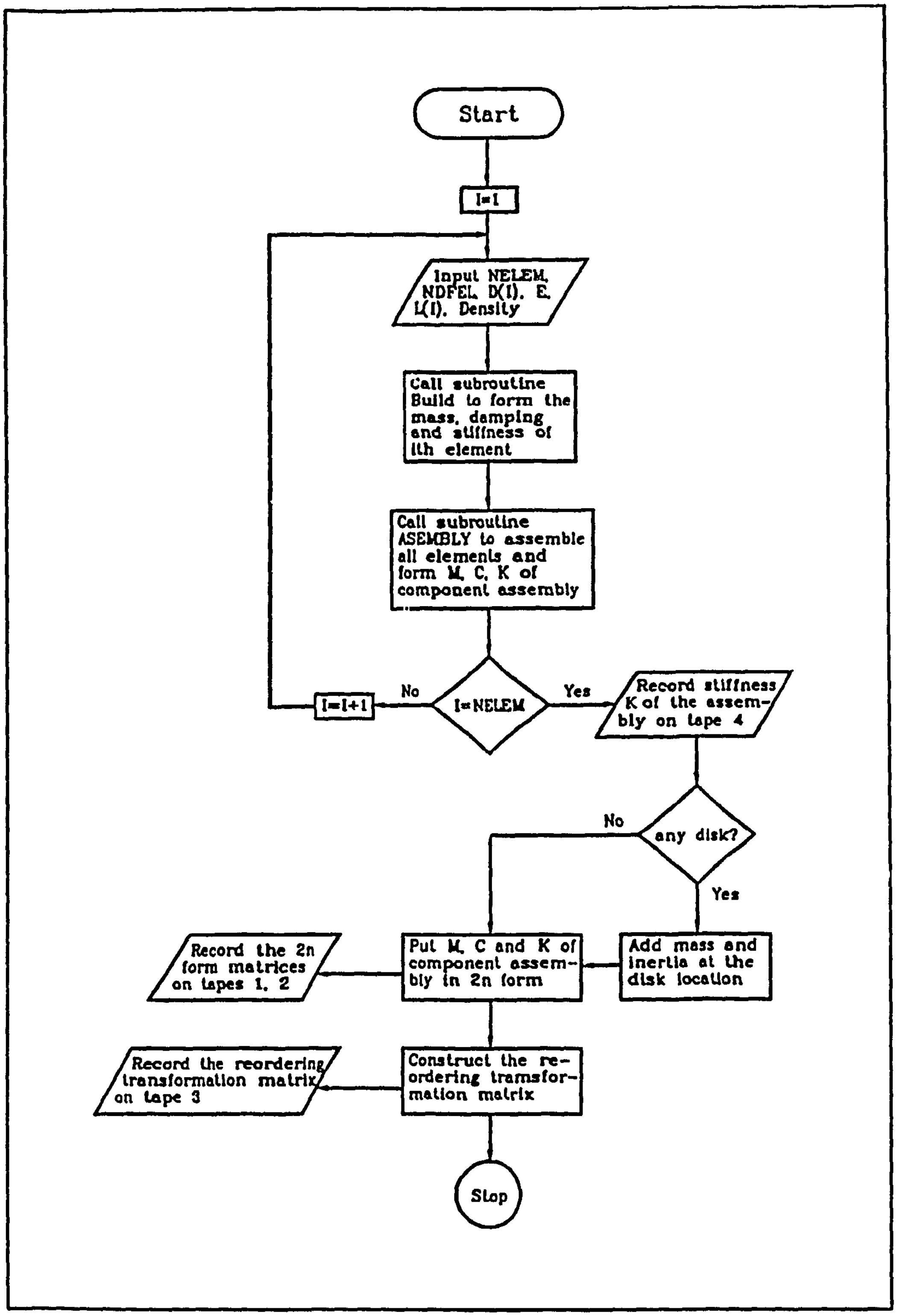

A. 3 Sub-Program CMS2

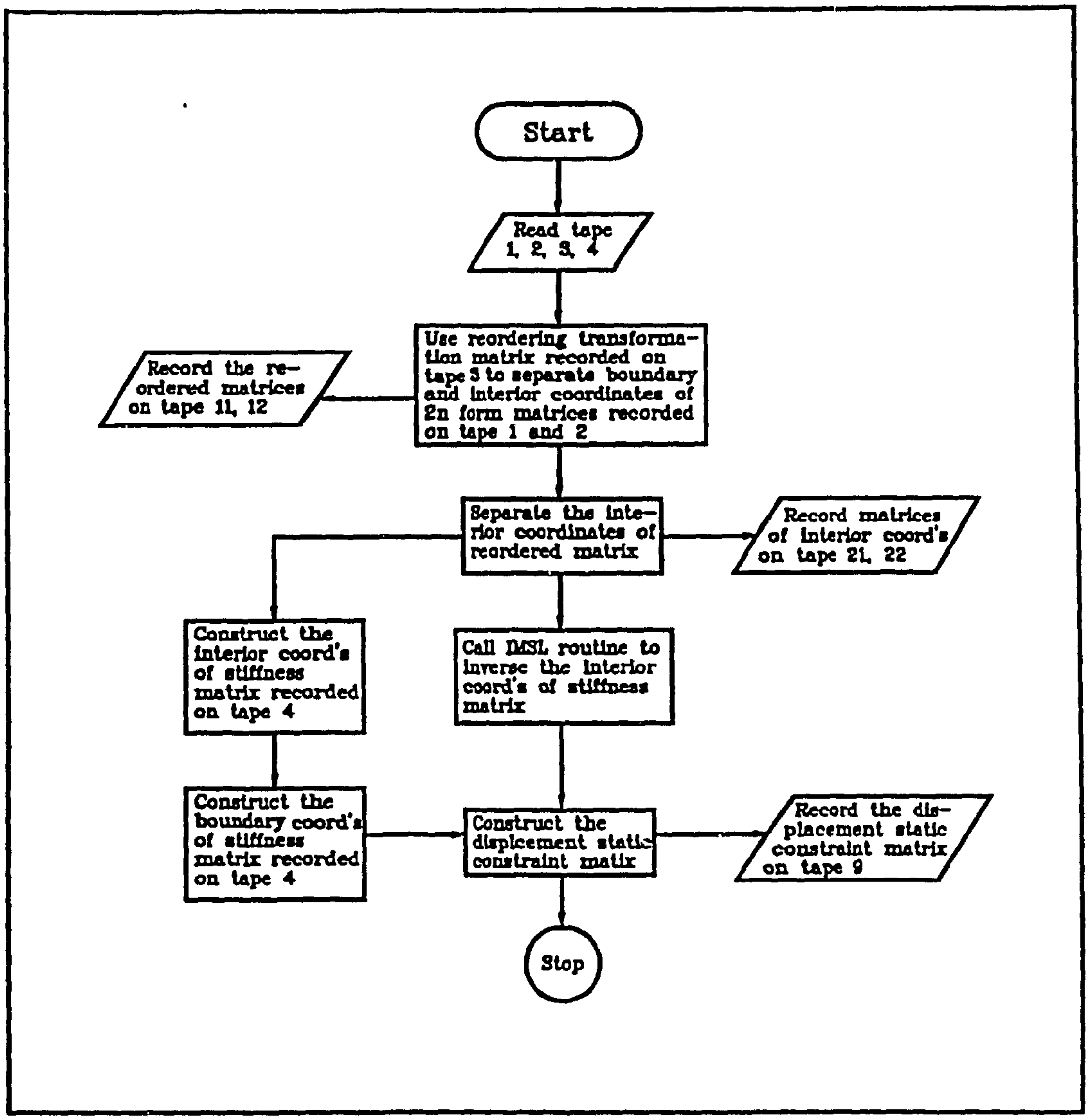

A. 4 Sub-Program CMS3

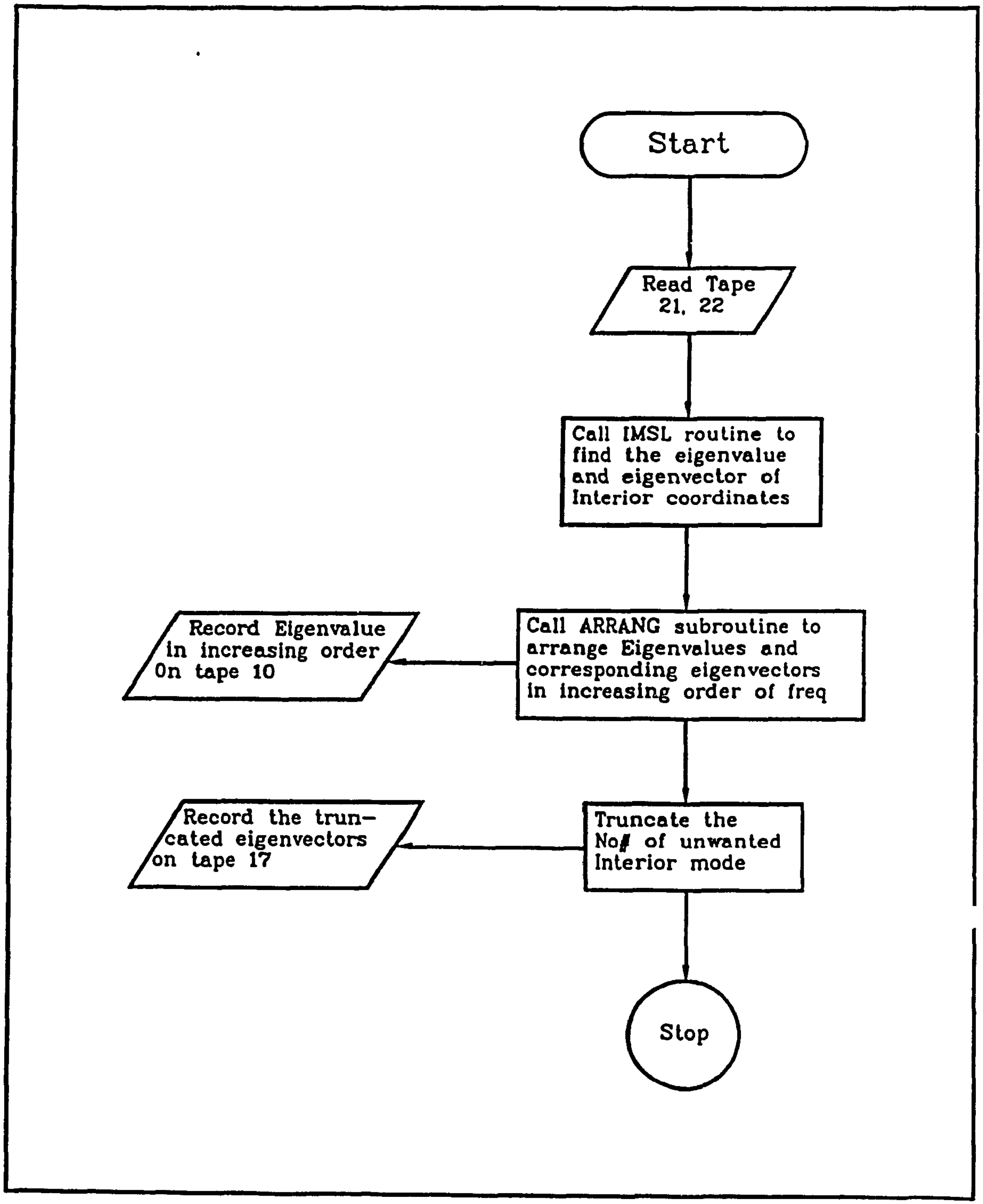

A. 5 Sub-Program CMS4

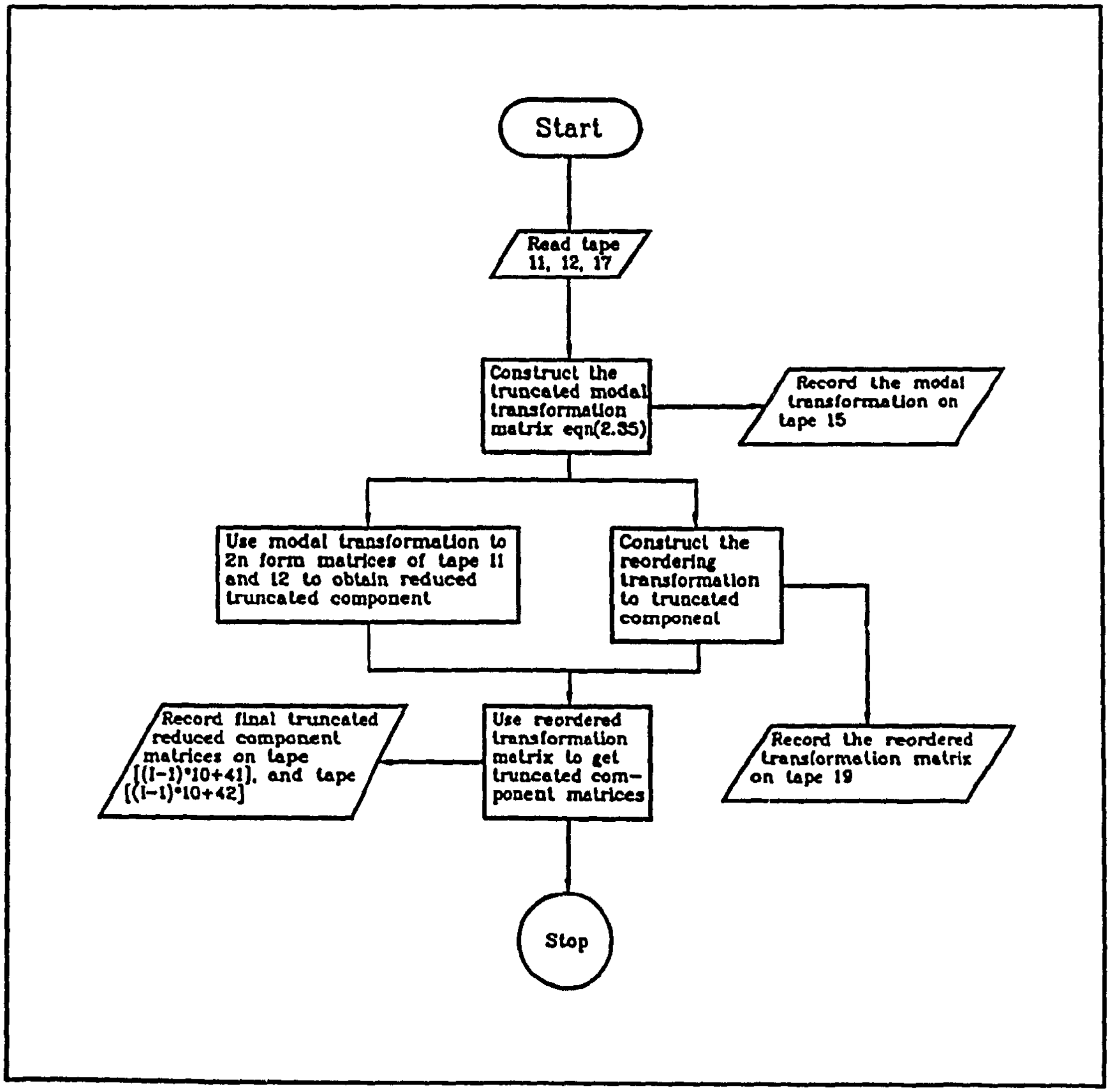

A. 6 Sub-Program CMS5

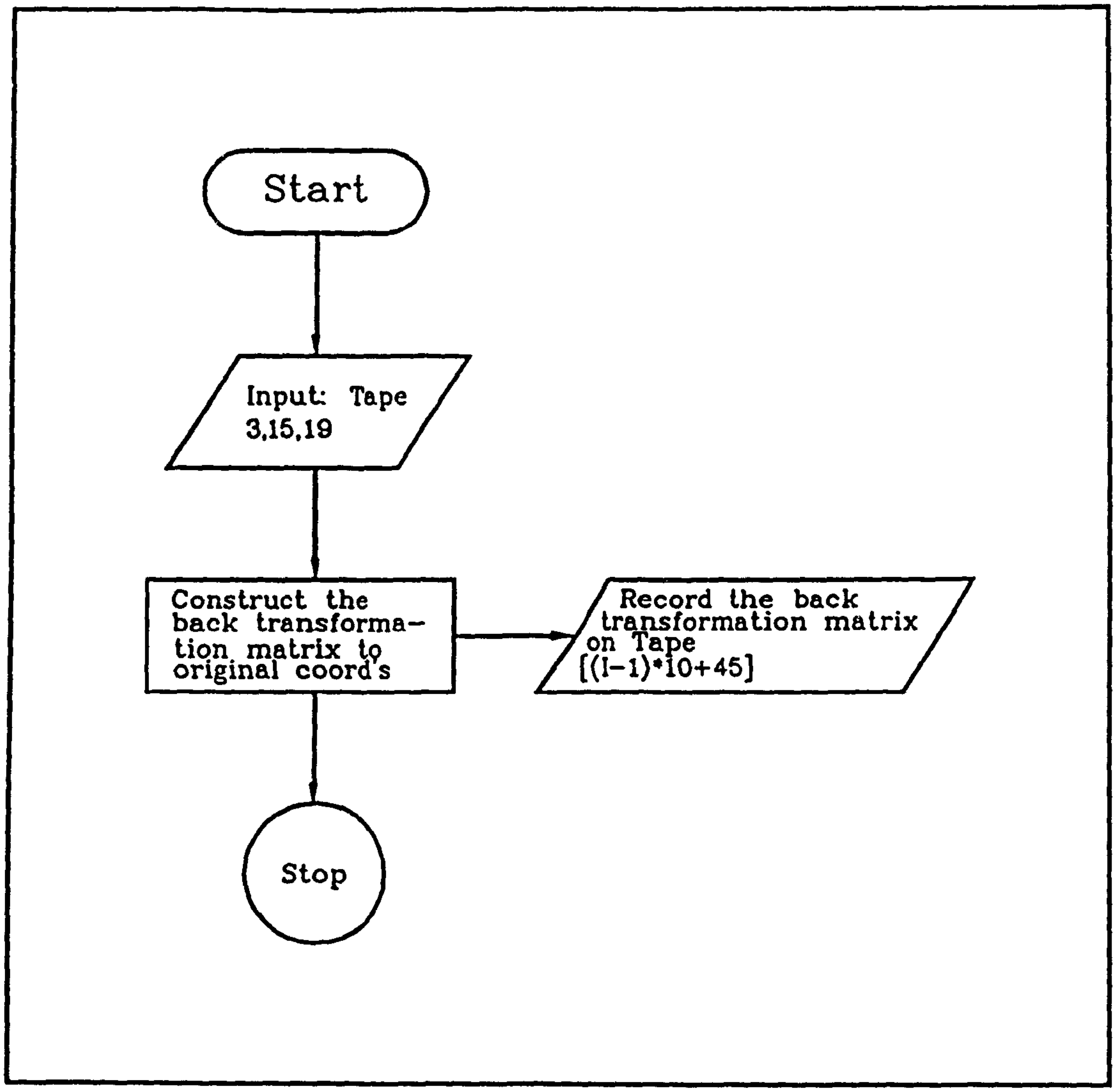

A. 7 Sub-Program CMSASS

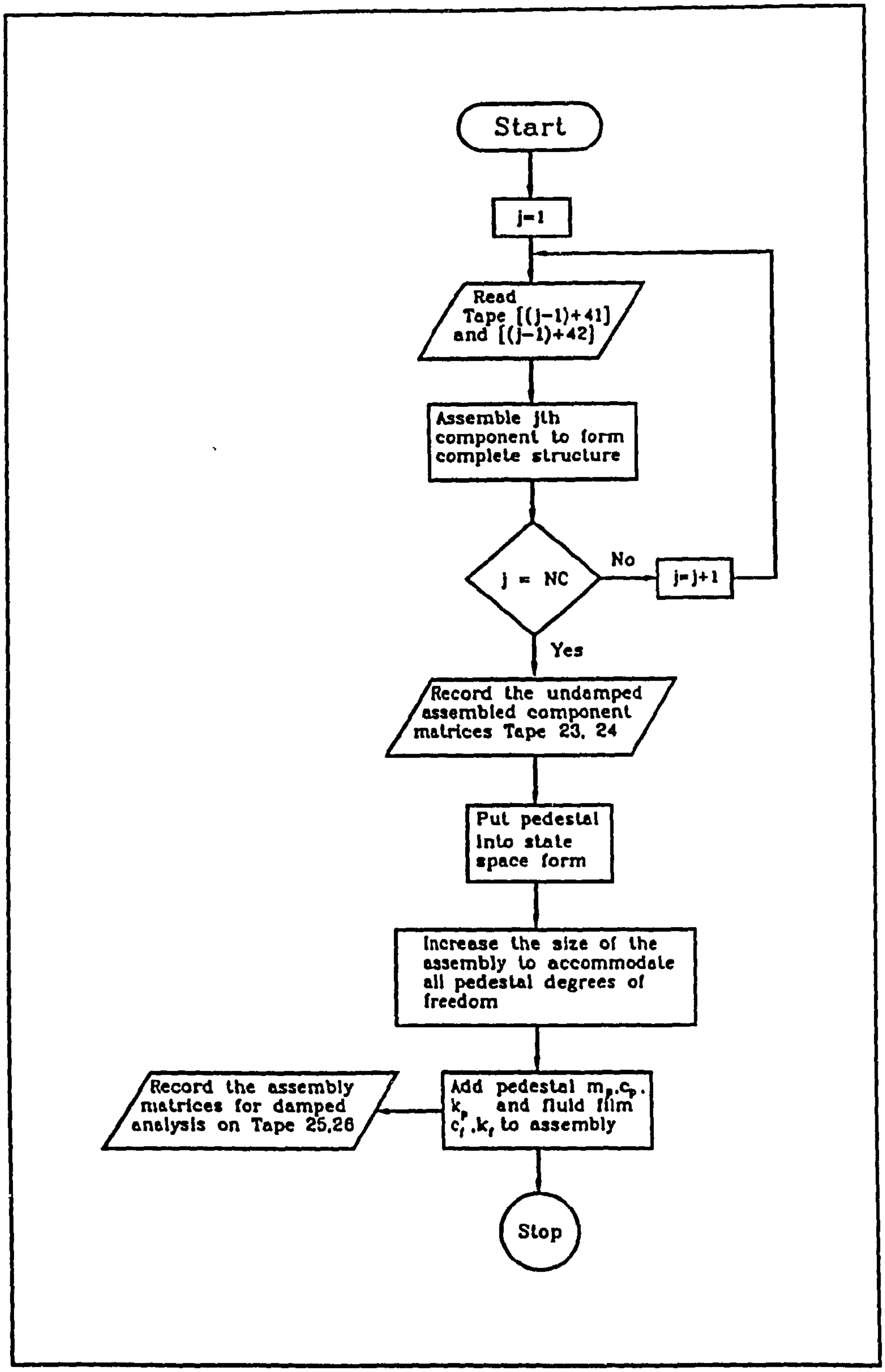

A. 8 Sub-Program CMSUND

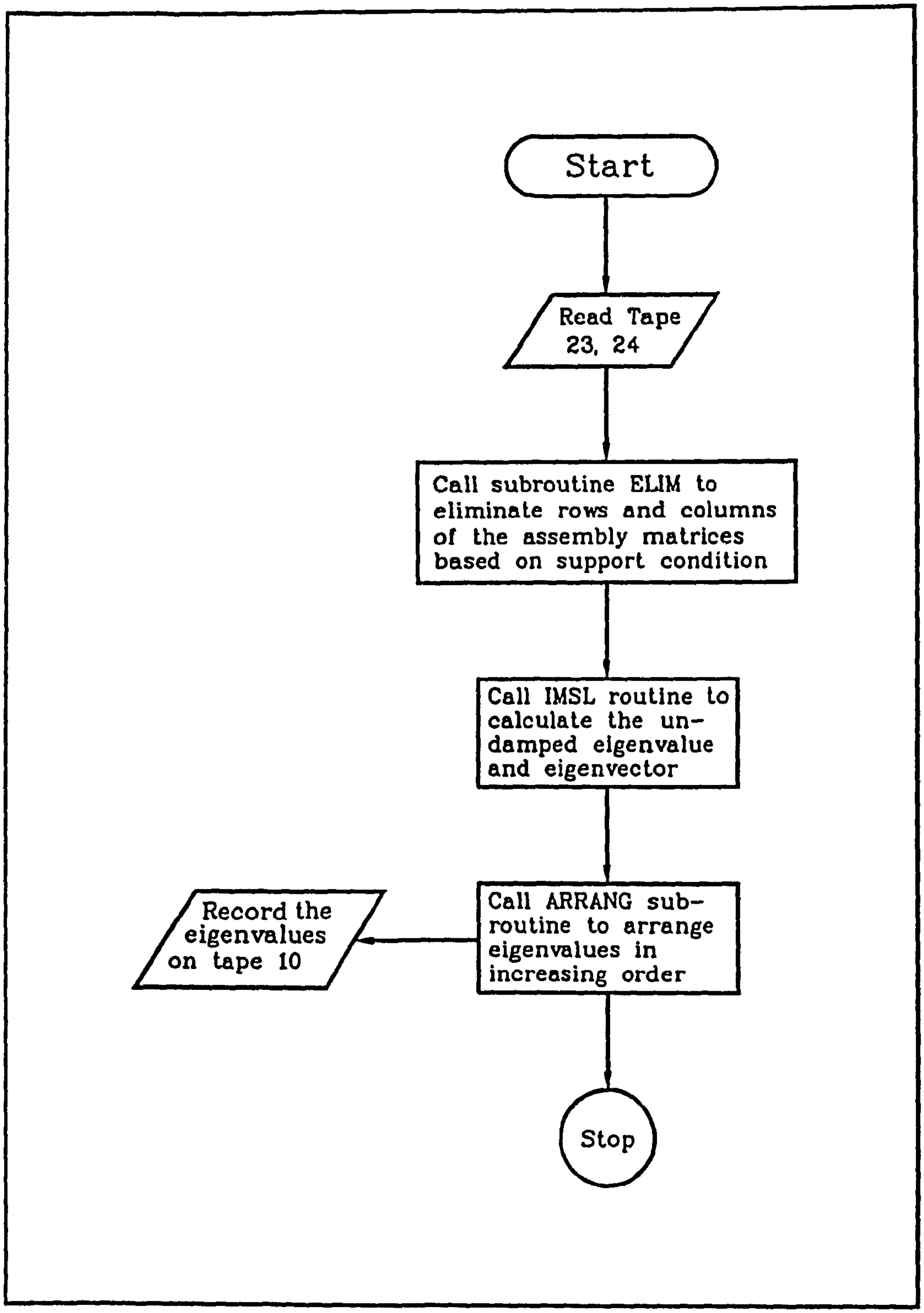

A. 9 Sub-Program CMSDAM

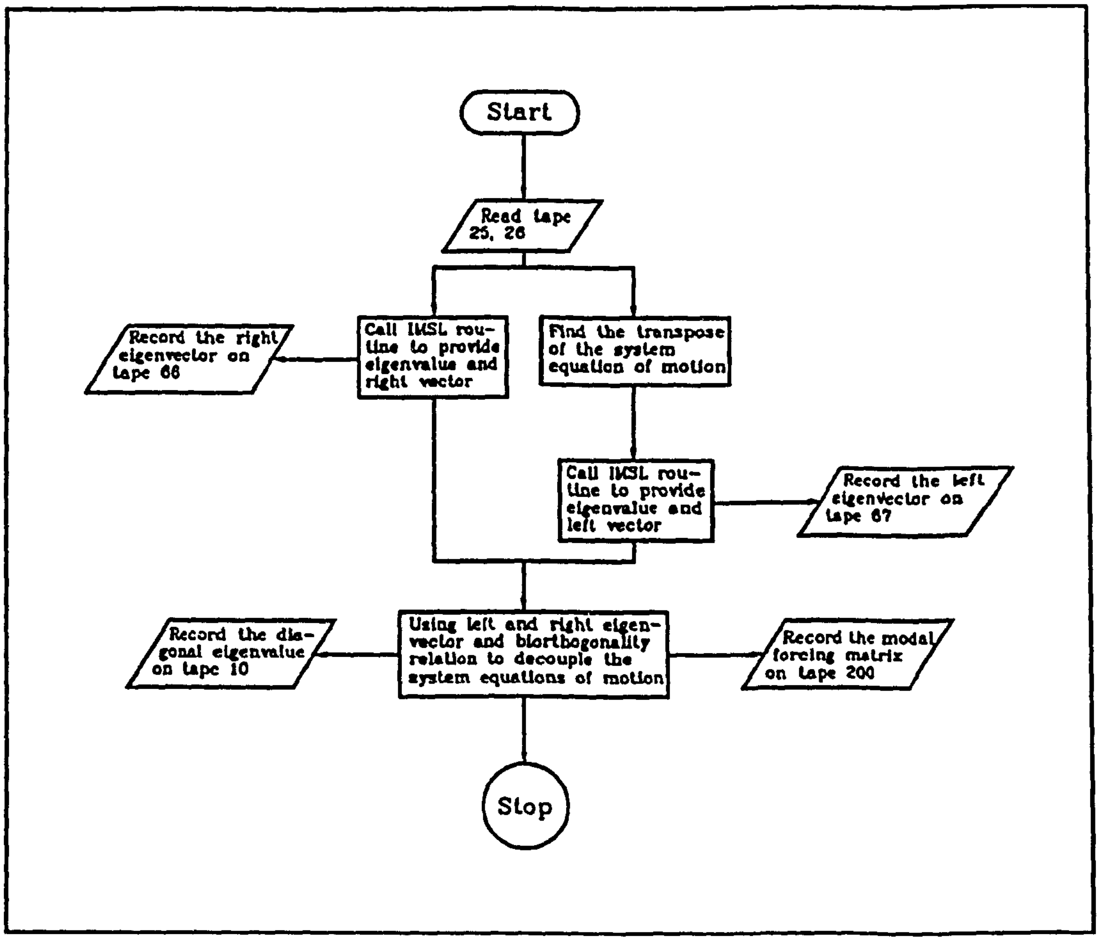

APPENDIX B

BEAM ELEMENT MATRICES

$$
\left[K_B^e \right] = \frac{EI}{\ell^3} \begin{bmatrix}
12 & & & & & & \text{symmetric} & \\
0 & 12 & & & & & & \\
0 & -6\ell & 4\ell^2 & & & & & \\
6\ell & 0 & 0 & 4\ell^2 & & & & \\
-12 & 0 & 0 & -6\ell & 12 & & & \\
0 & -12 & 6\ell & 0 & 0 & 12 & & \\
0 & -6\ell & 2\ell^2 & 0 & 0 & 6\ell & 4\ell^2 & \\
6\ell & 0 & 0 & 2\ell^2 & -6\ell & 0 & 0 & 4\ell^2
\end{bmatrix}
$$

$$
\left[M_r^e \right] = \frac{\mu D^2}{480\ell} \begin{bmatrix}
36 & & & & & & \text{symmetric} & \\
0 & 36 & & & & & & \\
0 & -3\ell & 4\ell^2 & & & & & \\
3\ell & 0 & 0 & 4\ell^2 & & & & \\
-36 & 0 & 0 & -3\ell & 36 & & & \\
0 & -36 & 3\ell & 0 & 0 & 36 & & \\
0 & -3\ell & -\ell^2 & 0 & 0 & 3\ell & 4\ell^2 & \\
3\ell & 0 & 0 & -\ell^2 & -3\ell & 0 & 0 & 4\ell^2
\end{bmatrix}
$$

$$
\left[M_t^e \right] = \frac{\mu\ell}{420} \begin{bmatrix}
156 & & & & & & \text{symmetric} & \\
0 & 156 & & & & & & \\
0 & 22\ell & 4\ell^2 & & & & & \\
22\ell & 0 & 0 & 4\ell^2 & & & & \\
54 & 0 & 0 & 13\ell & 156 & & & \\
0 & 54 & -13\ell & 0 & 0 & 156 & & \\
0 & 13\ell & -13\ell^2 & 0 & 0 & 22\ell & 4\ell^2 & \\
-13\ell & 0 & 0 & -3\ell^2 & -22\ell & 0 & 0 & 4\ell^2
\end{bmatrix}
$$